NEUROPATHOLOGY OF DUAL TRANSGENIC ALZHEIMER'S TYPE MICE FOLLOWING REPETITIVE MILD TRAUMATIC BRAIN INJURY

by

Rachel Barkey

A Thesis
Submitted to the
Graduate Faculty
of
George Mason University
in Partial Fulfillment of
The Requirements for the Degree
of
Master of Arts
Psychology

Committee:

_____ Director

_____

_____

_____ Department Chairperson

_____ Dean, College of Humanities and Social Sciences

Date: _____ Fall Semester 2020
George Mason University
Fairfax, VA

Neuropathology of Dual Transgenic Alzheimer's Type Mice Following Repetitive Mild Traumatic Brain Injury

A Thesis submitted in partial fulfillment of the requirements for the degree of Master of Arts at George Mason University

by

Rachel Barkey
Bachelor of Science
Messiah College, 2016

Director: Jane M. Flinn, Associate Professor
Psychology

Fall Semester 2020
George Mason University
Fairfax, VA

DEDICATION

This is dedicated to my family.

ACKNOWLEDGEMENTS

I would like to thank the member of my committee, Dr. Flinn, Dr. Murdock and Dr. Grant, for their help and guidance during this process.

A big thank you to Kristen Craven and Natalie Coshigano for letting me use the brains from their project, and to Caroline Neely and Carlos Hernandez for their invaluable knowledge of histological staining and quantification.

Finally, I would like to thank all of the mice, who so bravely sacrificed their lives in the name of science.

TABLE OF CONTENTS

LIST OF TABLES

LIST OF FIGURES

LIST OF ABBREVIATIONS

Alzheimer's Disease.....AD
Traumatic Brain Injury ..... TBI
Repetitive Mild Traumatic Brain Injury .....rmTBI
Transgenic..... tg
Activity of Daily Living..... ADL
Neurofibrillary Tangles..... NFTs
Amyloid Precursor Protein ..... APP
Medial Temporal Lobe ..... MTL
Entorhinal Cortex.....ERC
Glial Fibrillary Acidic Protein.....GFAP
Paired Helical Fragments..... PHF
Controlled Cortical Impact CCI

ABSTRACT

NEUROPATHOLOGY OF DUAL TRANSGENIC ALZHEIMER'S TYPE MICE FOLLOWING REPETITIVE MILD TRAUMATIC BRAIN INJURY

Rachel Barkey, M.A.

George Mason University, 2020

Thesis Director: Dr. Jane M. Flinn

Alzheimer's disease (AD) and Traumatic brain injuries (TBI) share many common pathological features and sustaining a TBI may increase the likelihood of developing AD later in life. Mild traumatic brain injuries are the most common form of TBI and once one injury occurs, the brain is more vulnerable to a second concussive impact. This study examined the effects of repetitive mild TBI (rmTBI) paradigm during adolescence on the deposition of amyloid and tau and neuronal loss in dual tg AD mice at 8 months of age. Mice were subjected to 5 mTBIs at 48-hour intervals at 3 months of age, then aged to 8 months for brain analysis. Amyloid deposition was measured through Congo Red staining. Thioflavin-S staining was performed to visualize tau tangles. Cresyl-Violet/Luxol Fast Blue staining was used to measure neuronal loss and white matter degeneration. rmTBI mice showed increased tangle formation in several cortical and hippocampal areas, while there were no differences in amyloid plaque formation.

There was decreased cell density in AD type mice in hippocampal regions, and increased cell density in AD mice in cortical regions compared to wildtype mice. rmTBI lead to lower cell density in motor and visual association cortex and infralimbic cortex. This study demonstrated that rmTBI in adolescence can progress AD pathology later in life.

CHAPTER ONE: INTRODUCTION

Alzheimer's disease (AD) is the most frequent cause of dementia, accounting for over 80% of dementia cases in the elderly worldwide (Bondi, Edmonds, and Salmon, 2017; Kumar, Singh, & Ekavali, 2015). The prevalence of AD is increasing and is expected to reach over 13 million cases by 2050 unless effective treatments are developed (Kumar et al., 2015). Currently, the only treatment options available target the symptoms rather than the underlying neuropathology. Pharmaceuticals that target neuropathology are failing in clinical trials (Kumar et al., 2015). Traumatic brain injury (TBI) is a known risk factor for AD (Faden & Loane, 2014; Lye & Shores, 2000; Tran, Laferla & Holtzman, 2011; Uryu, et al., 2002). It is therefore important to gain a greater understanding of the role that TBI plays in the development and progression of AD. The proposed study will examine the effects of repetitive mild traumatic brain injury (rmTBI) in adolescence on the deposition of amyloid and tau and neuronal loss in the infralimbic and hippocampal regions of 8-month-old duel transgenic (tg) hAPP/hTau mice.

Alzheimer's Disease Behavioral Changes and Neuropathology

AD leads to the progressive loss of episodic and semantic memory, as well as deficits in executive functioning, attention, language, and impairment of activities of daily living (ADLs) (Bondi et al., 2017). Neurologically, AD is defined by the presence of intracellular neurofibrillary tangles (NFTs) and extracellular plaques primarily

composed of amyloid protein (Braak & Braak, 1991; Hardy & Allsop, 1991; Hardy & Selkoe, 2002). White matter reductions, neuronal and vascular degeneration (Kumar et al., 2015; Nasrabady, Rizui, Goldman, & Brickman, 2018; Riechmann et al., 2016; Serrano-Pozo, Frosch, Masliah, & Hyman, 2011), destruction of dendritic spines and neuronal synapses (Kumar et al., 2015) and cortical atrophy (Serrano-Pozo et al., 2011) are also present in AD.

A main neuropathological feature of AD is the deposition of amyloid protein in the form of diffuse and neuritic plaques. The amyloid cascade hypothesis proposes that the primary neurological change leading to the deficits seen in AD is this deposition of amyloid-β protein (Aβ) (Hardy & Allsop, 1991; Hardy & Selkoe, 2002). Aβ is produced from the abnormal proteolytic cleavage of amyloid precursor protein (APP), a transmembrane protein (Haas & Selkoe, 1993; Hardy & Allsop, 1991; Hardy & Selkoe, 2002). Under nonpathological conditions, APP is cleaved by α-secretase, and does not lead to the production of a pathogenic form of Aβ. However, several genetic mutations have been found that lead to a preferential cleavage of APP by β- and γ- secretases. Proteolytic processing of APP by β- and γ- secretases leads to the formation of Aβ that can then aggregate into amyloid fibrils (Haas & Selkoe, 1993; Hardy & Selkoe, 2002). Intra- and extracellular signaling regulates APP metabolism and contributes to the production of Aβ (Haas & Selkoe, 2002). Irregular signaling results in an imbalance between the production and cleavage of Aβ, (Hardy & Selkoe, 2002; Kumar et al., 2015) which then spontaneously aggregate into soluble oligomers (Kumar et al., 2015). The most common Aβ oligomers found within senile plaques are Aβ40 and Aβ42 (Haas &

Selkoe, 2002; Serrano-Pozo et al., 2011). These oligomers coalesce to form insoluble β-pleated sheets which deposit as senile plaques (Kumar et al., 2015).

In AD, amyloid protein is most commonly found in the form of senile plaques. Senile plaques are composed of a central core of amyloid from which amyloid fibrils extend. Surrounding the plaque are dystrophic neural microglia and astrocytic processes (Hardy & Allsop, 1991; Serrano-Pozo et al., 2011). There are two main types of senile plaques: dense core and diffuse. In AD, diffuse plaques are found more frequently than dense core plaques, although diffuse plaques can also be found in cognitively intact individuals (Hardy & Allsop, 1991; Serrano-Pozo et al., 2011). Development of dense core plaques are thought to contribute to other neuropathological changes seen in AD, including dystrophic neurites, synaptic loss, neuron loss, and activation of astrocytes and microglia (Serrano-Pozo et al., 2011). In contrast, most diffuse plaques are not associated with dystrophic neurites or activation of glia (Hardy & Allsop, 1991). Diffuse plaques typically only develop into neuritic plaques in specific areas of the brain (Braak & Braak, 1991; Hardy & Allsop, 1991). The deposition of amyloid occurs in a stereotypical pattern, with deposition beginning in the medial temporal lobes (MTL) in the pre-subiculum and entorhinal cortex (ERC), eventually spreading throughout the cortical association areas while sparing the primary sensory and motor cortices. The hippocampus has relatively few amyloid deposits (Braak & Braak, 1991). Deposition of plaques in these areas disrupt synaptic connections and may lead to deficits seen in AD (Hardy & Selkoe, 2002) as the MTL are responsible for learning and memory (Bondi et al., 2017). However, although considered the main neurological change associated with AD, degree

of plaque deposition is not highly correlated with degree of behavioral deficits (Hardy & Selkoe, 1991).

Another main feature of AD neuropathology is tau deposition in the form of intracellular neurofibrillary tangles. Tau protein is essential for promoting microtubule assembly (Weingarten, Lockwood, Hwo, & Kirschner, 1975) and is found in AD as paired helical fragments (PHF) in NFTs and neuropil threads (Grundke-Iqbal et al., 1986; Hardy & Allsop, 1991; Serrano-Pozo et al., 2011). Neuropil threads are thought to be broken down dendrites and axons from neurons from neurites contained in NFTs (Serrano-Pozo et al., 2011). In AD, tau is abnormally hyperphosphorylated with NFTs primarily composed of both PHFs and abnormally folded and phosphorylated tau (Serrano-Pozo et al., 2011). As phosphorylation normally regulates the interaction of tau with other proteins, hyperphosphorylated tau may decrease normal interaction with other brain proteins, and lead to the formation of PHF (Grundke-Iqbal et al., 1986). PHFs then accumulate as tangles and in the neurites surrounding neuritic plaques (Grundke-Iqbal et al., 1986). Like amyloid, tau deposits throughout the brain in a stereotypical pattern, beginning with the CA1 region of the hippocampus and the subiculum, then spreading to the ERC and transentorhinal cortex. Eventually, tau spreads throughout cortical association areas with sparing of the primary sensory and motor cortices (Braak & Braak, 1991). Unlike amyloid, the amount and distribution of NFTs is highly correlated with the deficits seen in AD, as development first begins in the hippocampus and spreads to affect the entorhinal cortex, the sites of episodic and sematic memory (Braak & Braak, 1991; Bondi et al., 2017).

In addition to the development of senile plaques and NFTs, another neuropathological feature of AD is cortical atrophy. Cortical atrophy is primarily seen in the medial temporal lobes (Nasrabady, Rizvi, Goldman & Brickman et al., 2018; Rieckmann et al., 2016). Synapse and neuronal loss both contribute to cortical atrophy and follows the stereotyped pattern of NFT formation (Nasrabady et al., 2018). Dysregulation of oligodendrocytes leading to myelin loss and reduced white matter in the parahippocampus also contributes to cortical atrophy in AD (Nasrabady et al., 2018; Rieckmann et al., 2016). Neuronal degeneration, as seen by cell body and synapse loss as well as white matter degeneration occurs primarily in the MTL, correlating with behavioral deficits seen in AD (Serrano-Pozo et al., 2011).

Traumatic Brain Injury Behavioral Changes and Neuropathology

TBI is an alteration of brain function or evidence of brain pathology caused by an external force (Menon et al., 2010). Alterations of brain functioning may include a loss or change in level of consciousness, memory loss for events before or after injury, neurological deficits, and an alteration in mental state at the time of the injury (Menon et al., 2010). TBI is currently the leading cause of death for those under 25 and is predicted to become the third leading cause of death by 2050 (Popescu, Anghelescu, Daia, & Onose, 2015). In the US, 5 million people have a TBI related disability (Langlois, Rutland-Brown, & Wald, 2006). Although TBI are common, based on current diagnostic criteria, it is often difficult to recognize and diagnose mild TBI (mTBI), which accounts for 80% of reported brain injuries (Menon et al., 2010). However, adolescents and young adults are the mostly likely age group to experience TBI, with most of those injuries

occurring from contact sports or motor vehicle accidents (Bruns & Hauser, 2003; McKinley et al., 2009; Popescu et al., 2015). Only a small percent of sports related injuries results in a loss of consciousness, and as such will often go untreated and unreported, making data on mTBI is difficult to obtain (Langlois et al., 2006; Menon et al., 2010; Popescu et al., 2015). Almost one third of individuals who experience one TBI went on to have one or more additional injuries (McKinley et al, 2009). After the initial injury, the brain is more vulnerable to a second traumatic impact due to breakdown of the blood brain barrier and axonal injury (Laurer et al., 2001).

TBI leads to acute and chronic behavioral and psychological deficits, some of which are also seen in AD. In acute phases after TBI, young adults have difficulty with information processing, attention, memory, learning, sociality and behavior (Anderson, Brown, Newitt & Hoile, 2011). TBI may also lead to lifelong cognitive deficits such as depression and personality changes that manifest later in life (Faden & Loane, 2014; Langlois et al., 2006). Repetitive mild TBI (rmTBI) may lead to the development of chronic traumatic encephalopathy (CTE) which is linked to later onset of neuropsychiatric symptoms, including emotional lability, suicidal ideation, and aggressive behavior (Faden & Loane, 2014; McKee et al., 2009). Similar to AD behavioral symptoms of AD, rmTBI can also lead to deficits in attention, concentration, and memory, as well as confusion, disorientation and occasionally dementia (McKee et al., 2009).

Given the similar behavioral deficits, there have been several studies linking AD with TBI. An early study showed that the odds of a prior head injury were 5.31 times

higher in AD patients than in age-matched controls (Lye & Shores, 2000). Numerous studies have since attempted to link AD and TBI, however, these often have conflicting results due to difficulties with diagnosing AD and TBI (Faden & Loane, 2014; Langlois et al., 2006; Lye & Shores, 2000; Popescu et al., 2015). Along with recall bias of participants, a historic lack of consistency in the diagnosis and categorization of TBIs and difficulty of epidemiological studies having enough statistical power to find significance, there is still debate as to the extent that TBI contributes to AD (Lye & Shores, 2000). Even with these difficulties, it is well established that TBI is a risk factor for AD and other dementias later in life, however, the nature of the connection between the two is still unclear (Faden & Loane, 2014; Lye & Shores, 2014) necessitating further investigation into the mechanism underlying TBIs contribution to the progression of AD. A common neuropathological feature seen in both AD and TBI is increased level of tau protein. Levels of NFTs, total tau, and phosphorylated tau are all increased post injury (Faden & Loane, 2015; Johnson, Steward, & Smith, 2012; McKee et al., 2009; Roberts, Allsop, & Bruton, 1990; Tran et al., 2011). CTE is defined neurologically by an extensive deposition of phosphorylated tau (McKee et al., 2009). In humans, hyperphosphorylated tau increased after only one TBI (Faden & Loane, 2015). In mice, controlled cortical impact (CCI) TBI administration increased phosphorylated tau immunoreactivity 24 hours to 7 days post injury (Johnson et al., 2012). Studies of boxers with CTE show substantial tau tangles in the temporal lobe, which is where tangle formation is also seen in AD (McKee et al., 2009: Roberts et al., 1990). Specifically, abnormal total tau was seen in the fornix, amygdala, and CA1 regions after TBI (Tran et al., 2011). NFTs are

also increased in these areas in CTE (McKee et al., 2009). Extensive NFTs and thread-like neurites are seen throughout the brain in the dorsolateral frontal, insular, temporal, orbitolateral parietal, and inferior occipital cortices (McKee et al, 2009). Dense NFTs and ghost tangles are often seen in the hippocampus, ERC, and amygdala, often in greater density than those seen in AD (McKee et al., 2009). Even after a single TBI, a higher density and wider distribution of NFTs were seen in people one-year post-injury in the frontal gyrus and insular cortex, even in people as young as 27 years old (Faden & Loane, 2015; Johnson et al., 2012). NFTs were increased after one TBI and were found in the frontal gyrus and insular cortex (Faden & Loane, 2015; Johnson et al., 2012). Increased phosphorylated and total tau, as well as deposition of tau in these areas of the brain are also seen in AD, indicating that TBI can potentially initiate or accelerate the development of neurodegenerative disorders, as they have similar tau pathology.

The second neuropathological feature seen in both AD and TBI is the accumulation and deposition of amyloid. In CTE, amyloid plaques are seen in about one third of cases and are more frequently seen as diffuse plaques rather than the neuritic plaques of AD (McKee et al., 2009; Roberts et al., 1990). TBI increases amyloid and amyloid plaque formation even in younger individuals, occurring shortly after TBI and increases persisting after rmTBI for years after the initial injury. Increased Aβ pathology is also seen after one TBI in humans, with a trend toward a higher number of widespread plaques throughout the cortical region, particularly in the cingulate and superior frontal gyrus (Johnson et al., 2012). Aβ deposition and increased levels of insoluble Aβ was accelerated due to TBI, with rTBI leading to amyloidosis similar to that seen in AD

(Uryu et al., 2002). Expression of APP in the cortex is increased hours to years following TBI. Increased APP is seen both after a single hit and in a repetitive TBI model (Itoh et al., 2009). Animals that sustained rTBI had a significant increase in expression of APP up to 56 days post-injury, compared to animals that only received a single hit (Laurer et al., 2001). B-secretase, which leads to the amyloidogenic processing of APP and the formation of of toxic amyloid oligomers, is also more highly expressed following TBI (Blasko et al., 2004). Toxic amyloid oligomers, particularly Aβ42, is persistently increased following TBI and is thought to contribute to the long-term, progressive neurodegeneration cascades that result in amyloid plaques and NFTs (Faden & Loane, 2014). These changes in the level of expression of amyloid at several levels of processing may contribute to TBI, particularly rTBI, initiating or accelerating AD neurodegenerative pathways.

The final common neuropathological change seen in both AD and TBI is neuronal death and loss of white matter. A feature of CTE includes a reduction of brain weight due to the atrophy of the primary frontal temporal lobes, with some atrophy of the parietal lobes. There is also brain tissue scarring and neuronal loss present in the HC, ERC and amygdala (McKee et al., 2009). A traumatic impact can cause immediate mechanical injury and widespread neuronal death and can also initiate a delayed apoptotic process of surrounding tissues (Braun et al., 2017), which may be involved in TBI initiating long-term neurodegenerative processes (Jin et al., 2011). Delayed apoptosis is most commonly seen in the cerebral cortex and hippocampus (Braun et al., 2017). Chronic inflammation is induced by rmTBI and contributes to tissue atrophy and ongoing neurodegeneration

(Winston et al., 2015). Long term inflammation and microglia activation in the corpus callosum is present after TBI, which contributes to white matter degeneration. Survivors of TBI often show a loss of myelin and white matter atrophy several years after injury (Armstrong et al., 2016, Jin et al., 2011). Neuronal loss and white matter atrophy are thought to be an important factor linking TBI to the development and acceleration of AD (Armstrong et al., 2016; Jin et al., 2011; Winston et al., 2015,). However, several studies using animal models of TBI have failed to show neuronal and myelin loss after injury (Kane et al., 2011; Laurer et al., 2001; Mouzon et al., 2012). Neuronal and myelin degeneration may be an important link in the neuropathology of TBI and AD.

Experimental Models

The current study used a novel AD mouse model. Numerous mouse models of AD have been developed to mimic the neuropathological changes seen in humans with AD (McGowen, Eriksen & Hutton, 2006). Mice are genetically altered to induce changes to amyloid deposition by modifying amyloid precursor protein (APP), presenilin 1 (PSEN1) and presenilin 2 (PSEN2) genes (McGowen et al., 2006). Alterations of these genes lead to an increased expression of the amyloidogenic pathways through the proteolytic processing of APP with β- and γ-secretase (McGowen et al., 2006). PS1 and PS2 mutations lead to the development of early onset AD (Dia, Zheng, & Zhang, 2017). Mouse models to express human tau have also been developed to produce NFTs and neuropil threads (McGowen et al., 2006). Tau mouse models often display the structural and biochemical features of human NFTs; typically, these mice also show neuronal loss in the affected brain regions (McGowen et al., 2006). Mice have been developed that

express both amyloid and tau pathology. The most used model is the 3xTg mouse which contains the $PSEN1_{m146v,}$ APP_{SWE} and MAPT(P301L) mutations, which express amyloid and tau, along with the gene for early onset AD (McGowen et al., 2006). Lippi et al. (2018) developed a mouse model that expresses human amyloid and human tau without the addition of an early onset gene (Lippi, Smith, & Flinn, 2018), as early onset AD only accounts for a 5-10% of AD cases (Dia et al., 2017). This mouse model contains the Swedish (K670N/M6716) and Indiana (V717F) mutations to APP as well as the MAPT(P301L) tau mutation by crossing the J20APP model with the rtg4510(P301L) model (Lippi et al., 2018).

As well as a novel mouse model, this study also used a modified CCI TBI paradigm. There are several TBI designs for animal models, ranging from severe to mild injury as well as a single hit versus multiple injuries (Kane et al., 2011; Laurer et al., 2001; Mouzon et al., 2012; Xiong, Mahmood, & Chopp, 2013. The fluid percussion injury models involved exposing the dura then setting a pendulum to strike a piston in a fluid reservoir that causes a fluid pressure pulse to hit the exposed dura (Xiong et al., 2013). This technique briefly displaces and deforms the brain. Injury severity is controlled by the strength of the pressure pulse. However, there is little biomechanical control of the insult, as only the pendulum is adjustable (Xiong et al., 2013). This model also has a high mortality rate. Another model is the blast TBI model. Blast TBI models are used to replicate blast injuries that occur to military personnel where there is brain injury due to a shock wave but no external injuries (Xiong et al., 2013). Blast TBIs are administered using a compression driven shock wave tube. Blast injuries typically show

different pathology than other TBI models (Xiong et al., 2013). In weight drop TBI models, the skull is exposed, and the injury occurs through a free-falling guided weight. Adjusting the weights and the height of the drop can change the severity of the injury. Maramou's weight drop injury model has been modified to induce repetitive injuries (Xiong et al., 2013). This model does not require scalp incisions and mice spontaneously recover their righting reflex. In CCI TBI models a pneumatic or electromagnetic impact device is used to drive a rigid impactor onto exposed dura. This model can cause widespread degeneration in cortical, hippocampal, and thalamic regions (Xiong et al., 2013). The current study modified the CCI method of TBI by administering a closed head injury to be able to administer multiple hits and maintain a low mortality rate, as well as adding a platform that dropped the mouse when the hit occurred to mimic rotational effects seen in TBI.

This study examined the effects of a rotational CCI rmTBI paradigm during adolescence on the deposition of amyloid and tau and neuronal loss in dual tg AD mice at 8 months of age. Amyloid deposition was measured through Congo Red staining. Thioflavin-S staining was performed to visualize tau tangles. Cresyl-Violet/Luxol Fast Blue staining was used to measure neuronal loss and white matter degeneration. It is expected that mice subjected to rmTBI during adolescence will have higher levels of amyloid plaque and tau tangle formation, as well as more advanced neuronal loss and white matter degeneration.

CHAPTER TWO: METHODS

Subjects

Wildtype, P301L (rTg4510), and hAPP (J20) mice were obtained from Jackson Laboratory for breeding purposes at George Mason University's Krasnow Institute for Advanced Study Animal Lab. Twelve female rTg 4510 mice were bred with six male J20 mice to produce hAPP/rTG4510 double transgenic mice that express both human amyloid and human tau. One male J20 mouse was paired with two female rTg4510 for a period of two weeks. Before pups were born mothers were moved to individual cages and mothers were housed individually with their litter until pups were weaned. Weaning occurred when pups were between 21 and 38 days old. After weaning, mice were housed according to sex in rat cages. Females were housed 2-6 per cage and males were housed 2-4 per cage. Mice were provided with enrichment in their home cages throughout the duration of the study, including an "igloo", a running wheel, and a NylaBone for chewing. Food and water were provided *ad libidum* and light were kept on a 12-hour light/dark cycle.

At 11-21 days old, tail snips of a maximum of 2mm were taken from each mouse and sent to Transnetyx for genotype determination. Only wildtype and hAPP/rTg4510 mice were used for this study. Mice without these genotypes were used as littermates.

Overall, a total of 55 mice were bred for the larger study that this project is a part of. 25 hAPP/rTg4510 mice and 30 wildtype mice were separated into groups receive rmTBI (Tg: n = 12 wt: n = 16) and sham mice (Tg: n = 13 wt: n = 14). For this study, 20

mice (n = 5 per group) were aged to 8 months. At 8 months of age, mice were euthanized with carbon dioxide and cervical dislocation via guillotine. Brains were removed, flash frozen with dry ice, and stored at -80^{o}C until staining.

rmTBI Administration

TBI was administered using a modified Lecia ImpactOne Controlled Cortical Impact (CCI) device with a dropping platform. Mice began TBI administration at 8 weeks of age. TBI administrations occurred over 10 days, with a 48-hour interval between each hit for a total of 10 hits.

Mice were first anesthetized with isoflurane until unresponsive to a paw or tail pinch. Mice were positioned under the CCI device so that the impact occurred between the bregma and lambda at the middle of the skull with continued isoflurane administration through a nose cone. Once correctly positioned, the mouse was removed from anesthesia and hit with a 5mm CCI device tip with an impact depth of 5mm and a force of 3 m/s. When the hit was administered, the platform supporting the mouse dropped, mimicking rotational effects and acceleration and deceleration forces present in human TBI. In concussion, acceleration and deceleration forces, particularly rotational acceleration and deceleration are thought to be important for the damage seen following head injury (McKee et al., 2009

Mice were monitored after hit, and time-to-righting and time-to-ambulation were measured. Sham animals also underwent anesthesia and placed on the device platform with no hit. Sham animals were also monitored for time-to-righting and time-to-

ambulation. Before being placed in the home cage, animals were monitored for signs of neurological damage.

Histology

Fresh frozen brain tissue was sliced at 16µm and mounted onto charged slides (SuperFrost Plus Slides, Fisher Scientific) using a Leica CM3050S cryostat. Slices were taken from the infralimbic region of the frontal cortex at ~ bregma 1.39mm which is anterior to the injury site (Figure 1). Slices posterior to the site of injury were taken from the early hippocampus at ~1.34mm past bregma (Figure 2), middle hippocampus at ~2.54mm past bregma (Figure 3) and the late hippocampus at ~2.80mm past bregma (Figure 4). From early hippocampal slices the primary motor and primary somatosensory cortex, the secondary somatosensory cortices, and the hippocampus were analyzed. From middle hippocampal slices hippocampal regions CA1, CA3, and dentate gyrus (DG) were analyzed along with the entorhinal and perirhinal and the parietal association cortices. From late hippocampal slices, CA1, CA3, DG, temporal association cortex and visual association cortex were analyzed. Slices were stained with either Luxol Fast Blue/Cresy Violet, Congo Red, or Thioflavin S according to the following protocols.

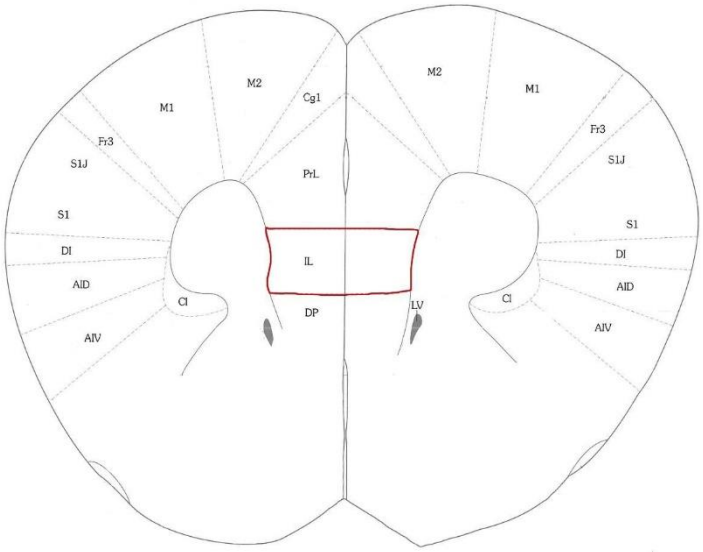

Figure 1: Quantified Section of Infralimbic Region.
Quantification of each histological stain was performed on the infralimbic regions (IL) outlined in red. Image modified from Franklin & Paxinos (2008).

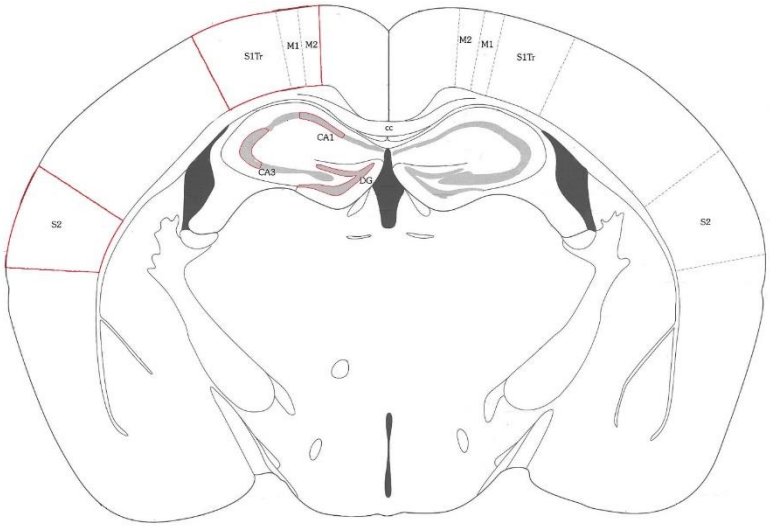

Figure 2: Quantified Sections of Early Hippocampal and Cortical Regions.
Quantification of each stain was performed on the early hippocampal and cortical regions highlighted in red including the DG, CA1 and CA3 regions of the hippocampus, the motor (M1, M2) and primary somatosensory cortices and the secondary somatosensory cortex. Image modified from Franklin & Paxinos (2008).

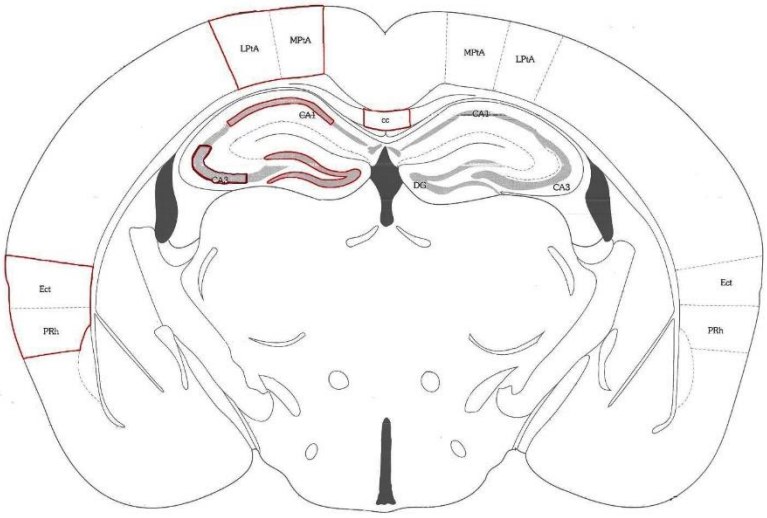

Figure 3: Quantified Sections of Middle Hippocampal and Cortical Regions. Quantification of each stain was performed on the middle hippocampal and cortical regions highlighted in red, including the DG, CA1, CA3, entorhinal (Ect) and perirhinal cortices (PRh), and parietal association cortices (LPtA, MPtA). Image modified from Franklin & Paxinos (2008).

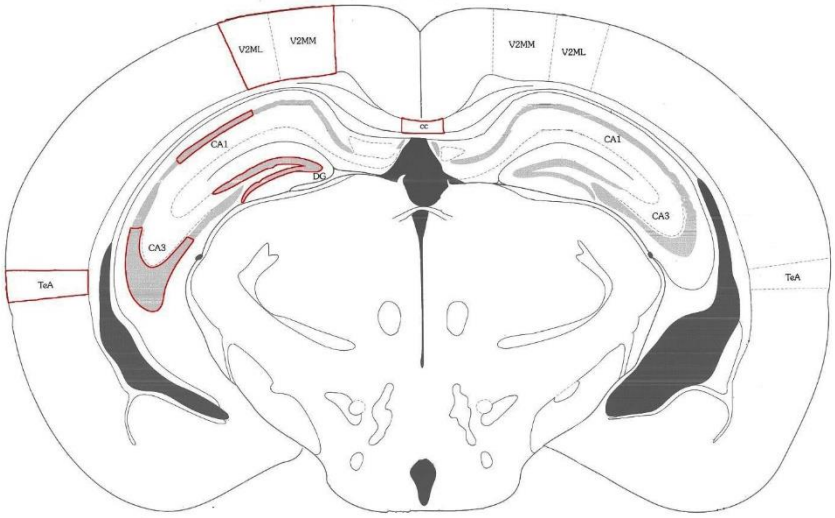

Figure 4: Quantified Sections of Late Hippocampal and Cortical Regions. Quantification of each stain was performed on the late hippocampal and cortical regions highlighted in red, including the DG, CA1, CA3, temporal association cortex (TeA) and visual association cortex (V2ML, V2MM). Image modified from Franklin & Paxinos (2008).

Thioflavin-S

NFTs were assessed using a thioflavin-S staining protocol modified (Sun, Nguyen, & Bing, 2002) and used previously in our lab. Slides were post-fixed in 4% PFA for 8 minutes, as modified by Sun et al. 2002 and then washed with PBS and placed into a 0.25% potassium permanganate solution for 4 minutes. Slides were placed in a 1% sodium borohydride solution, washed with distilled water, and placed in a 0.05% thioflavin-S in 50% ethanol solution for 8 minutes. Tissue samples were differentiated in two washes of 80% ethanol followed by three washes of distilled water, then incubated with 10x PBS for 30 minutes at 4^{o}C. Imaging was completed using a microscope with a FITC cube attachment with a magnification of 40x, green levels of 1.26, and a consistent exposure time of approximately 1 second. Image J software obtained from NIH was used to overlay images in order to intensify the tangles for visualization purposes; tangles were also counted using Image J software.

Congo Red

The HT-60 Congo Red Staining Kit (Sigma-Aldrich) was used to visualize insoluble amyloid plaques. Tissue slides were placed in Mayer's hematoxylin solution (Sigma-Aldrich) for 2 minutes, rinsed in distilled water for 5 minutes and placed in alkaline sodium chloride for 20 minutes following by staining in Congo Red solution for 30 minutes. Slides were rinsed in ethanol, cleared in xylene for 3 minutes and coverslipped with DPX. Slides were left overnight to dry before imaging. Plaques were then counted.

Luxol FastBlue/Cresyl-Violet

Luxol Blue/ Cresyl violet stain was used to determine neuronal structure and to assess neuronal damage. Sections were brought to room temperature and then dehydrated in two washes of 100% ethanol and 95% ethanol, incubated overnight in 0.1% filtered Luxol blue solution at 37ºC in a humidity chamber. The next day, the samples were rinsed with 95% ethanol and distilled water, then differentiated with 0.05% lithium carbonate, two washes of 70% ethanol and two rinses with distilled water. Differentiation was completed four times for each slide, rinsed with 70% ethanol and distilled water, then incubated in warmed, filtered 0.1% cresyl violet solution at 37ºC in a humidity chamber for 30 minutes. Samples were then dehydrated in two washes of 95% and 100% ethanol for one minute and then cleared with two washes of xylene for 3 minutes. Slides were coverslipped with DPX mountant and left to dry overnight before imaging.

CHAPTER THREE: RESULTS

Thioflavin-S

A t-test was performed between AD SHAM and AD TBI mice to assess number and size of tau tangles. In the IL, AD TBI mice had significantly more tau tangles ($\bar{x}$ = 249.10, SEM = 20.29) than AD SHAM mice ($\bar{x}$ = 163.50, SEM = 16.44, $t(8) = -3.28$, p = 0.011). No significant difference in size of tau tangles was found ($p = 0.347$).

In cortical regions, AD mice subjected to TBI had significantly more tau tangles in the parietal association cortex ($\bar{x}$ = 316.56, SEM = 26.22, $\bar{x}$ = 131.00, SEM = 5.16, $t(8) = -6.94$, $p = 0.002$), the entorhinal and perirhinal cortex ($\bar{x}$ = 270.98, SEM = 16.69, $\bar{x}$ = 146.38, SEM = , w13.11, $t(8) = -5.87$, $p < 0.001$) and the visual association cortex ($\bar{x}$ = 191.97, SEM = 25.89, $\bar{x}$ = 92.30, SEM = 9.06, $t(8) = -3.63$, $p < 0.015$). Average values presented as (AD TBI, AD SHAM), respectively. No significant differences were found in the primary and secondary motor cortex ($p = 0.225$), secondary somatosensory cortex ($p = 0.093$), or temporal association cortex ($p = 0.120$).

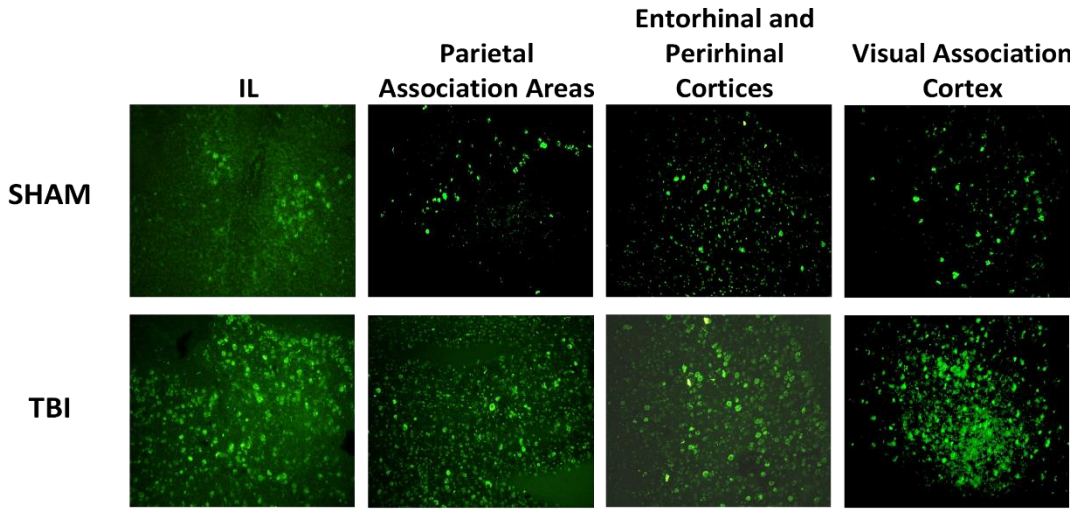

Figure 5: Thioflavin-S Staining in Cortical Regions of AD brains.
Fluorescent staining with thioflavin-S revealed AD brains subjected to rmTBI have significantly more tau tangle formation in the infralimbic region of the prefrontal cortex the medial and lateral parietal association cortices, the entorhinal and perirhinal cortices, and visual association areas compared to AD brains that did not receive rmTBI

In hippocampal regions, AD mice had significantly greater number of tangles in the mid DG ($\bar{x}$ = 89.60, SEM = 7.33, $\bar{x}$ = 54.83, SEM = 11.57, $t(8) = -2.54$, $p = 0.035$), mid CA1 ($\bar{x}$ = 105.07, SEM = 8.33, $\bar{x}$ = 52. 30, SEM = 12.02, $t(8) = -3.61$, $p = 0.007$), late DG ($\bar{x}$ = 98.27, SEM = 5.66, $\bar{x}$ = 54.27, SEM = 4.83, $t(8) = -5.91$, $p < 0.001$), and late CA1 ($\bar{x}$ = 86.53, SEM = 9.01, $\bar{x}$ = 52. 70, SEM = 9.53, $t(8) = -2.58$, $p = 0.033$) compared to AD sham mice. Average values presented as (AD TBI, AD SHAM),

respectively. No significant differences were found between groups in the number of tau tangles present in the early HC (p = 0.210), mid CA3 (p = 0.080) or late CA3 (p = 0.674).

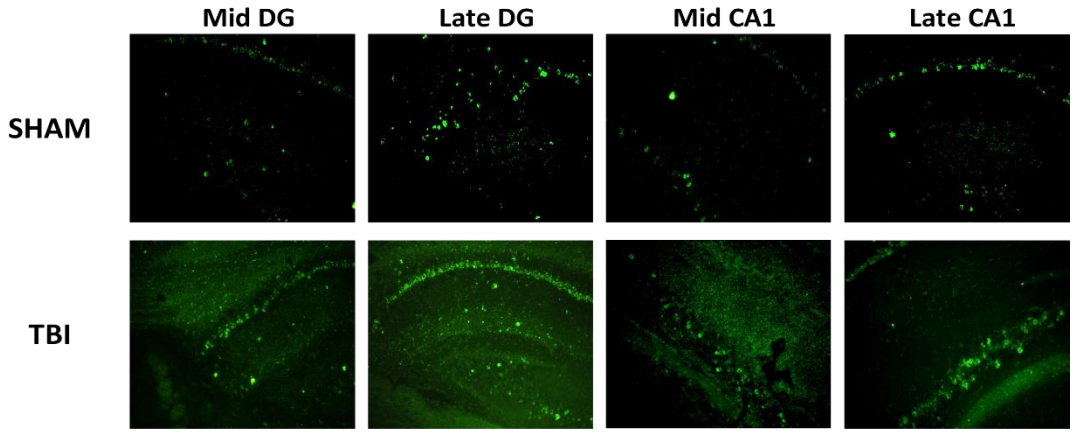

Figure 6: Thioflavin-S Staining in Hippocampal Regions of AD brains.
Fluorescent staining with thioflavin-S revealed AD brains subjected to rmTBI have significantly more tau tangles in the mid DG, late DG, mid CA1, and late CA1 of the hippocampus compared to AD type brain that did not receive rmTBI.

There was a significant main effect of size of tau tangles in the temporal association cortex ($\bar{x}$ = 2258.7 pixels, SEM 172.93; $\bar{x}$ = 1708.9 pixels, SEM = 162.15t(8) = -2.31, p = 0.049) with AD TBI mice having significantly larger tangles than AD sham mice. Average values presented as AD TBI, AD SHAM, respectively. No significant difference of size of tau tangles was found in other brain regions assessed.

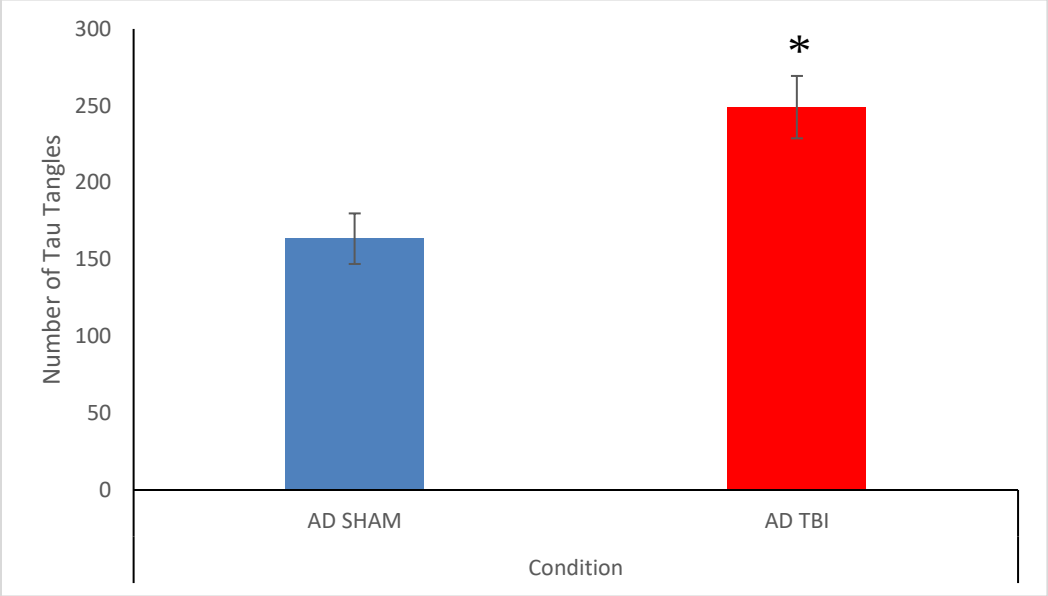

Figure 7: Number of Tau Tangles in the Infralimbic Region.
Average number of tau tangles (±SEM) found in the infralimbic region of the prefrontal cortex of AD TBI and AD sham mice. AD mice subjected to rmTBI had significantly more tau tangles than sham mice ($p = 0.012$). * indicates significance at $p < 0.05$ level.

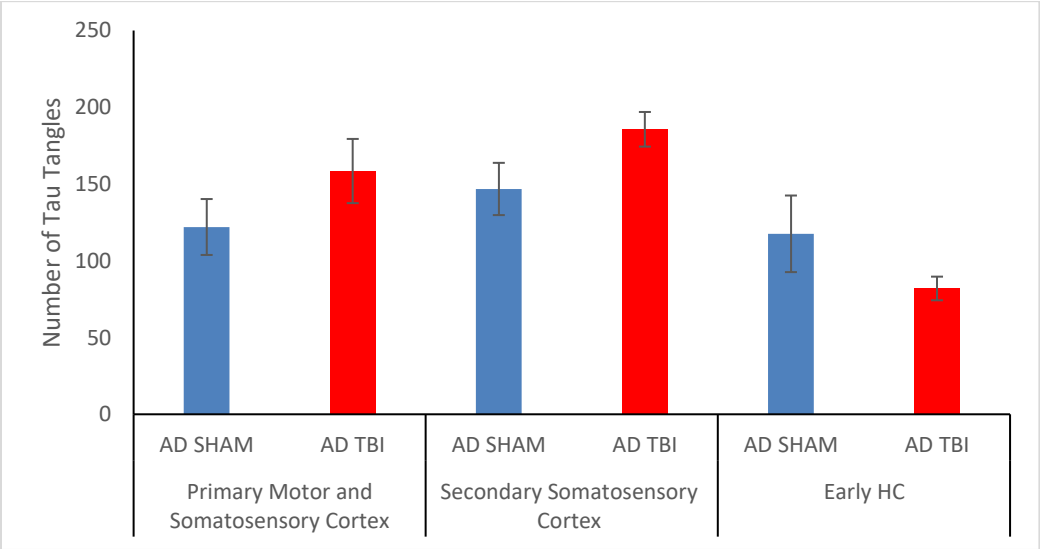

Figure 8: Number of Tau Tangles in Early Cortical and Hippocampal Regions.
Average number of tau tangles (±SEM) found in early hippocampus and cortical regions of AD sham and AD TBI mice. There are no significant differences between TBI and

sham mice in the primary motor and somatosensory cortex (p = 0.099), the secondary somatosensory cortex (p = 0.209), or the early hippocampus (p = 0.072).

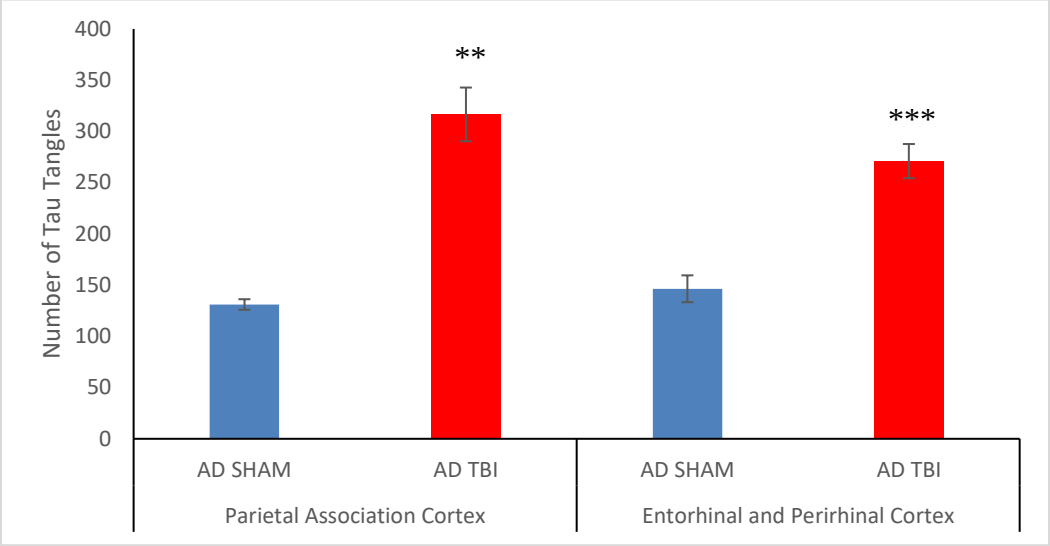

Figure 9: Number of Tau Tangles in Mid Cortical Regions.
Average number of tau tangles (±SEM) found in mid cortical regions. AD TBI mice had significantly more tau tangles than AD sham mice in the parietal association cortex (p = 0.002) and in the entorhinal and perirhinal cortices (p < 0.001). ** indicates significance at p < 0.01 level, *** indicates significance at p < 0.001 level

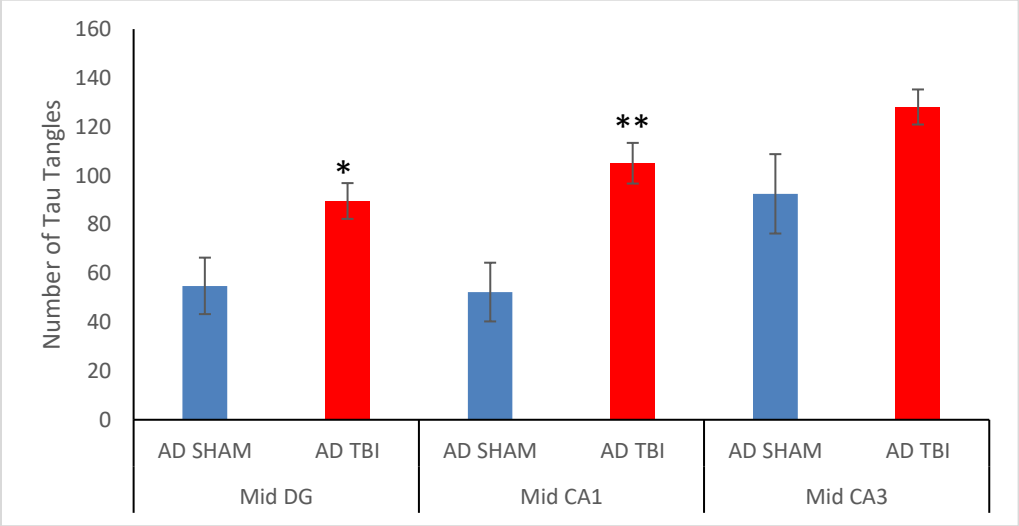

Figure 10: Number of Tau Tangles in Mid Hippocampal Regions.
Average number of tau tangles (±SEM) found in mid hippocampal regions. AD TBI mice had significantly more tau tangles than AD sham mice in the mid DG (p = 0.04) and the

mid CA1 (p = 0.008) but not in the mid CA3 (p = 0.120). * indicates significance at p < 0.05 level, ** indicates significance at p < 0.01 level.

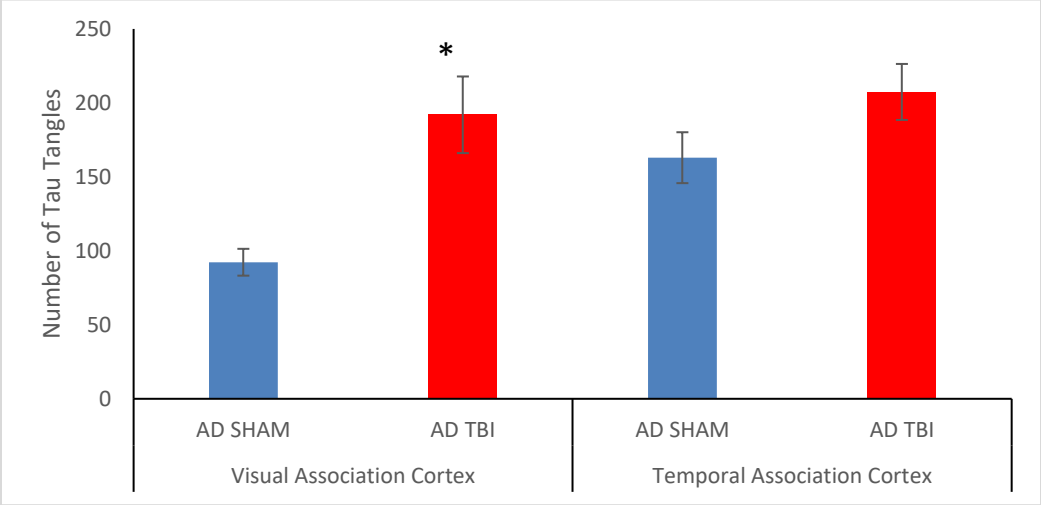

Figure 11: Number of Tau Tangles in Late Cortical Regions.
Average number of tau tangles (±SEM) found in late cortical regions. AD TBI mice had significantly more tau tangles than AD sham mice in the visual association cortex (p = 0.015), but not in temporal association cortex (p = 0.121). *** indicates significance at p < 0.001 level.

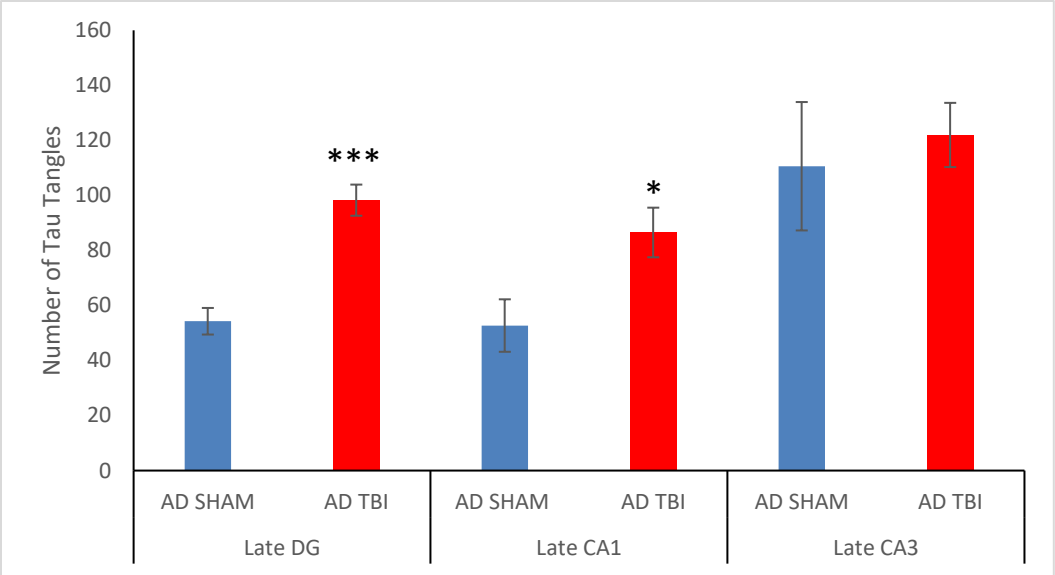

Figure 12: Number of Tau Tangles in Late Hippocampal Regions.
Average number of tau tangles (±SEM) found in late hippocampal regions. AD TBI mice had significantly more tau tangles than AD sham mice in the late DG (p < 0.001) and the

late CA1 ($p = 0.033$) but not in the late CA3 ($p < 0.97$). * indicates significance at a $p < 0.05$ level, *** indicates significance at $p < 0.001$ level.

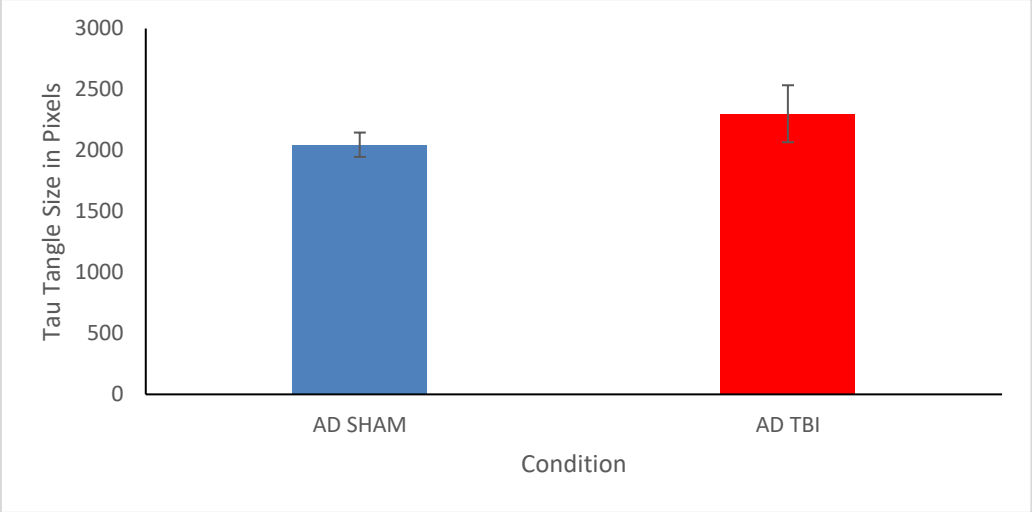

Figure 13: Tau Tangle Size in the Infralimbic Region.
Average size of tau tangles (±SEM) found in the infralimbic region of the prefrontal cortex of AD TBI and AD sham mice. There was no significant difference of tangle size found between AD TBI and AD sham mice ($p = 0.360$).

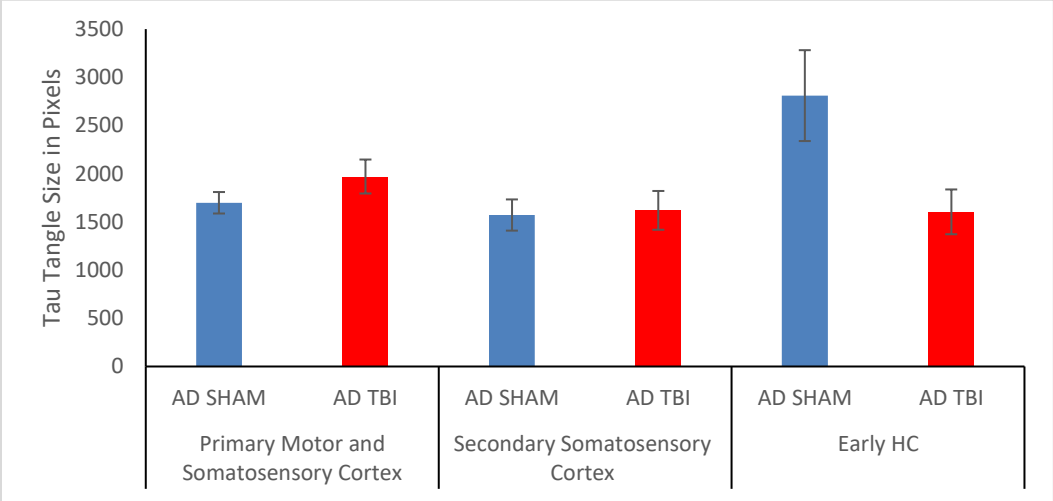

Figure 14: Tau Tangle Size in Early Hippocampal and Cortical Regions.
Average size of tau tangles (±SEM) found in early hippocampus and cortical regions of AD sham and AD TBI mice. There are no significant differences between TBI and sham

mice in the primary motor and somatosensory cortex (p = 0.234), the secondary somatosensory cortex (p = 0.856), or the early hippocampus (p = 0.063).

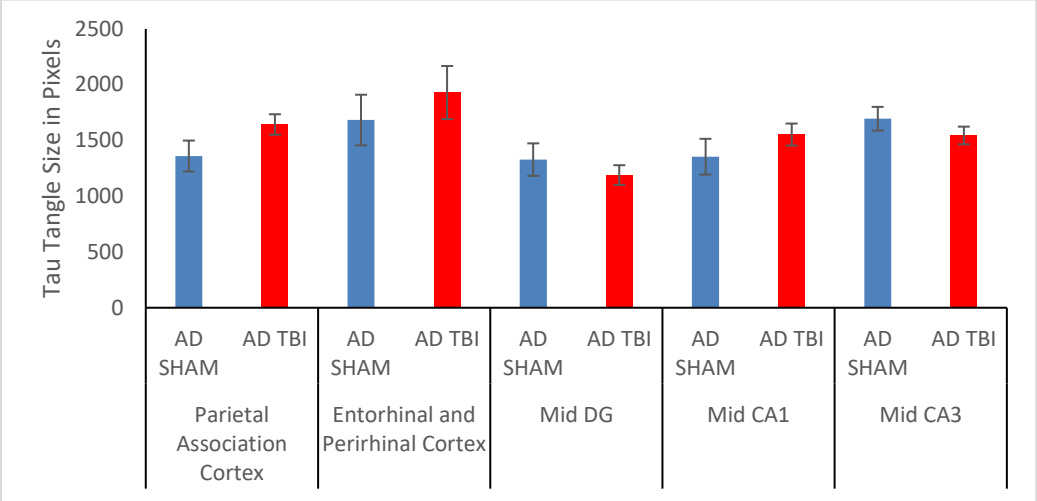

Figure 15: Tau Tangle Size in Mid Cortical and Hippocampal Regions.
Average size of tau tangles (±SEM) found in mid cortical and hippocampal regions. There was no significant difference of tangle size found between AD TBI and AD sham mice in the parietal association cortex (p = 0.133), entorhinal and perirhinal cortices (p = 0.475), mid DG (p = 0.445), the mid CA1 (p = 0.329) or the mid CA3 (p = 0.293).

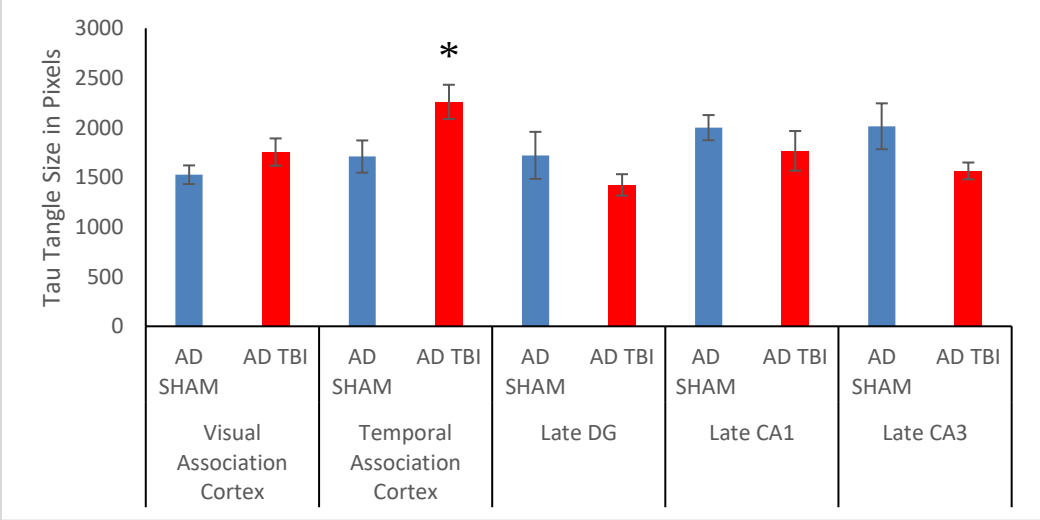

Figure 16: Tau Tangle Size in Late Cortical and Hippocampal Regions.
Average size of tau tangles (±SEM) found in late cortical and hippocampal regions. AD TBI mice had significantly more tau tangles than AD sham mice in the temporal association cortex (p = 0.049) but not in the visual association cortex (p = 0.212). There was no significant difference of tangle size found between AD TBI and AD sham mice in

the late DG ($p = 0.300$), late CA1 ($p = 0.218$) or late CA3 ($p = 0.126$). * indicates significance at $p < 0.05$ level.

Congo Red

A t-test was performed between AD sham and AD TBI mice to assessed number of amyloid plaques. No significant differences were found in any brain regions assessed. There was no significant difference in number of amyloid plaques between AD TBI and AD sham mice in cortical regions, specifically the infralimbic region ($p = 0.790$), the primary motor and somatosensory cortices ($p = 0. 157$), secondary somatosensory cortex, parietal association cortex ($p = 0.258$), entorhinal and perirhinal cortex ($p = 0.374$), visual association cortex ($p = 0.795$) or the temporal association cortex.

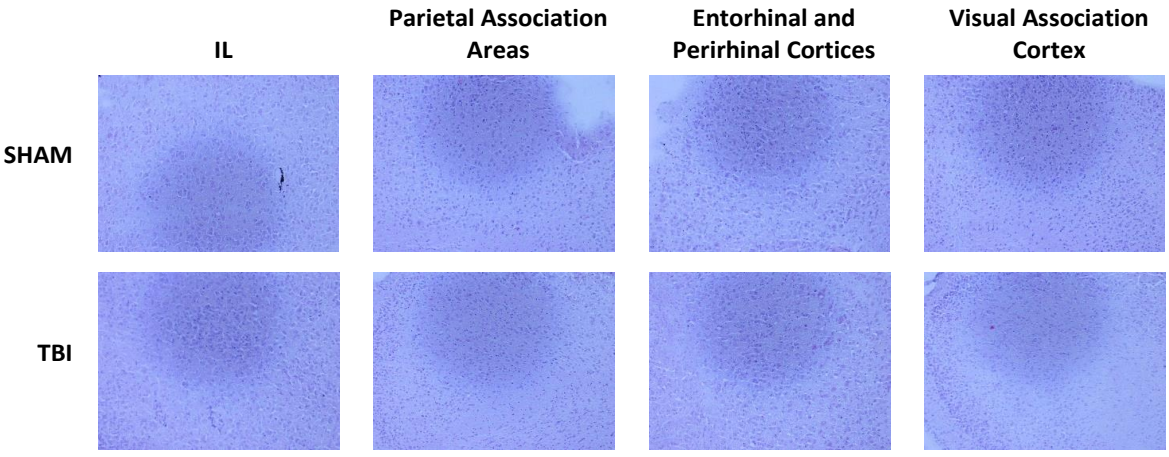

Figure 17: Congo Red Staining for Amyloid Plaques in Infralimbic and Cortical Regions.
Congo red staining for amyloid plaques revealed no significant difference between AD TBI and AD SHAM mice in number of amyloid plaques in the cortical regions assessed ($p > 0.05$), even in areas where there was significantly more tau tangle formation.

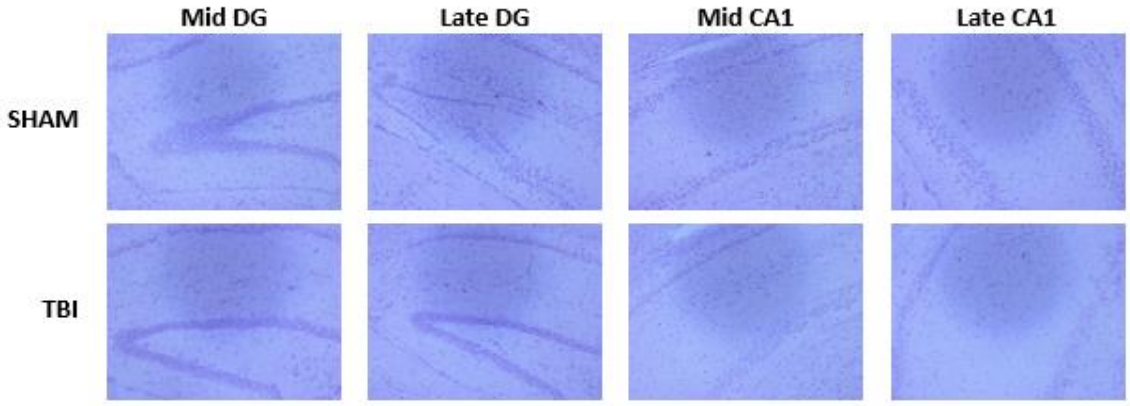

Figure 18: Congo Red Staining for Amyloid Plaques in Hippocampal Regions.
Congo red staining for amyloid plaques revealed no significant difference between AD TBI and AD SHAM hippocampal areas ($p > 0.05$), even in areas where there was a significant difference in tau tangle formation.

Luxol FastBlue/Cresyl-Violet

A 2x2 ANOVA was performed between WT TBI, WT sham, AD TBI, and AD sham mice to assess cell body and white matter density. In late hippocampal slices, there was a main effect of genotype at midline corpus collosum on white matter density ($F(1,16) = 8.389$, $p = 0.011$) with wt mice showing significantly greater white matter density than AD type mice. No significant differences were found in the white matter density of the corpus callosum at midline in early hippocampal slices ($F(3, 16) = 2.988$, $p = 0.062$) or in mid hippocampal slices ($F(3, 16) = 1.078$, $p = 0.386$). Cell density at midline corpus callosum was also assessed. There were no significant differences found in cell density in the early corpus callosum ($F(3, 16) = 0.337$, $p = 0.799$), the mid corpus

callosum ($F(3,16) = 0.956$, $p = 0.437$) or the late corpus callosum ($F(3, 16) = 0.576$, $p = 0.639$).

In the infralimbic regions, a main effect of genotype was present ($F(1, 16) = 5.291$, $p = 0.035$) where AD mice have significantly greater cell density than wt mice. A genotype*condition interaction was present ($F (1, 16) = 15.126$, $p = 0.001$) with AD TBI mice expressing greater cell density than wt TBI mice.

In cortical regions, a genotype effect was found in the secondary somatosensory cortex ($F (1, 16) = 5.792$, $p = 0.029$) and in the primary and secondary motor cortex ($F (1, 16) = 6.967$, $p = 0.018$) where AD type mice have significantly higher cell density than wt mice. A main effect of condition was found in the primary and secondary motor cortex ($F (1, 16) = 4.778$, $p = 0.044$) and in the visual association cortex ($F (1, 16) = 6.166$, $p = 0.024$) with mice who received TBI displaying significantly lower cell density than sham mice. There were no significant differences in cell density found in the parietal association cortex ($F (3, 16) = 1.473$, $p = 0.260$), the entorhinal and perirhinal cortex ($F(3, 16) = 0.845$, $p = 0.489$) or in the temporal association cortex ($F(3, 16) = 2.482$, $p = 0.098$).

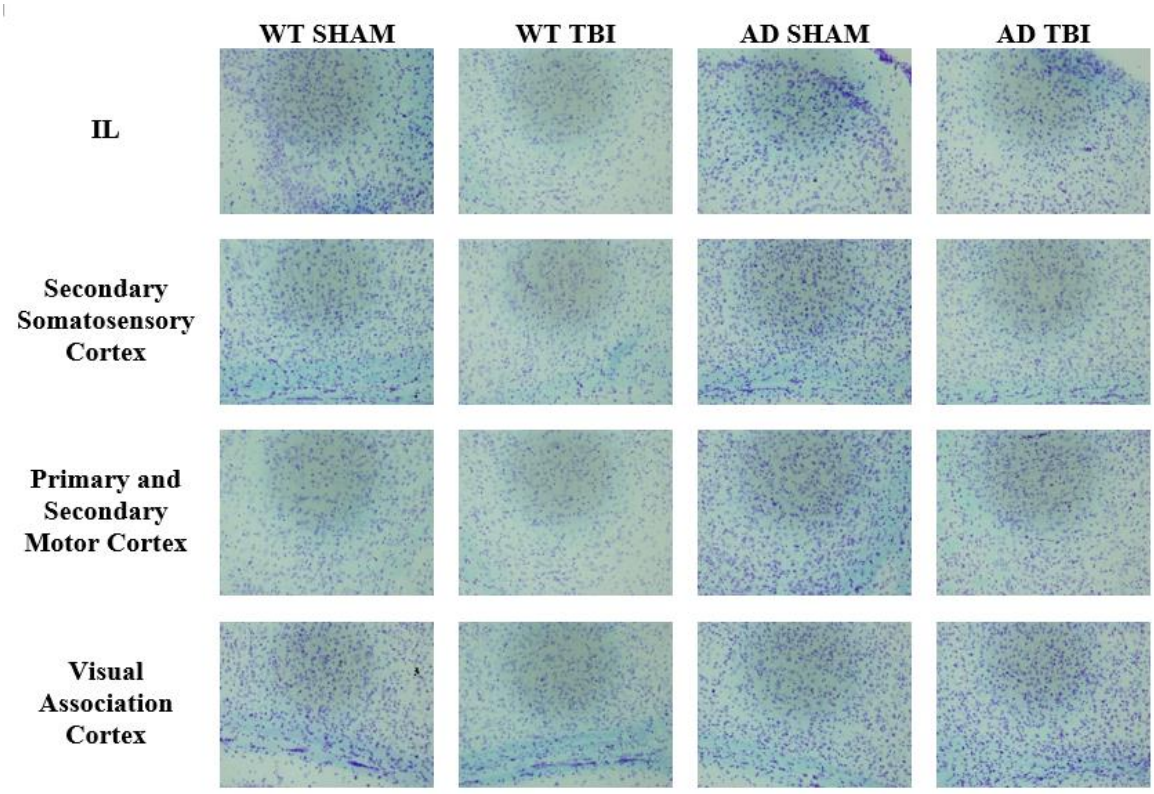

Figure 19: Cresyl-Violet Staining for Cell Bodies in Infralimbic and Cortical Regions.
Cresyl-violet staining for cell bodies revealed greater cell density in AD mice than wt mice ($p = 0.035$), and in AD TBI mice than wt TBI mice ($p = 0.001$) in the infralimbic region. Significantly greater cell density was seen in AD mice than wt mice in the secondary somatosensory ($p = 0.029$) and primary and secondary motor cortex ($p = 0.018$). Mice who received TBI has significantly lower cell density in the primary and secondary motor cortex ($p = 0.04$) and in the visual association cortex ($p = 0.024$).

In hippocampal regions, a main effect of genotype was found in the early HC ($F(1, 16) = 5.214$, $p = 0.036$), the mid DG ($F(1, 16) = 124.959$, $p < 0.001$), mid CA1 ($F(1, 16) = 21.667$, $p < 0.001$), late DG ($F(1, 16) = 186.021$, $p < 0.001$), and late CA1 ($F(1, 16)$

= 21.982, $p < 0.001$) where AD type mice have significantly lower cell density than wt mice. This result is opposite of what is found in cortical regions, where AD mice have greater cell density. No significant differences of cell density were found in the mid CA3 ($F(3, 16) = 0.967$, $p = 0.432$) or late CA3 ($F(3, 16) = 0.714$, $p = 0.558$).

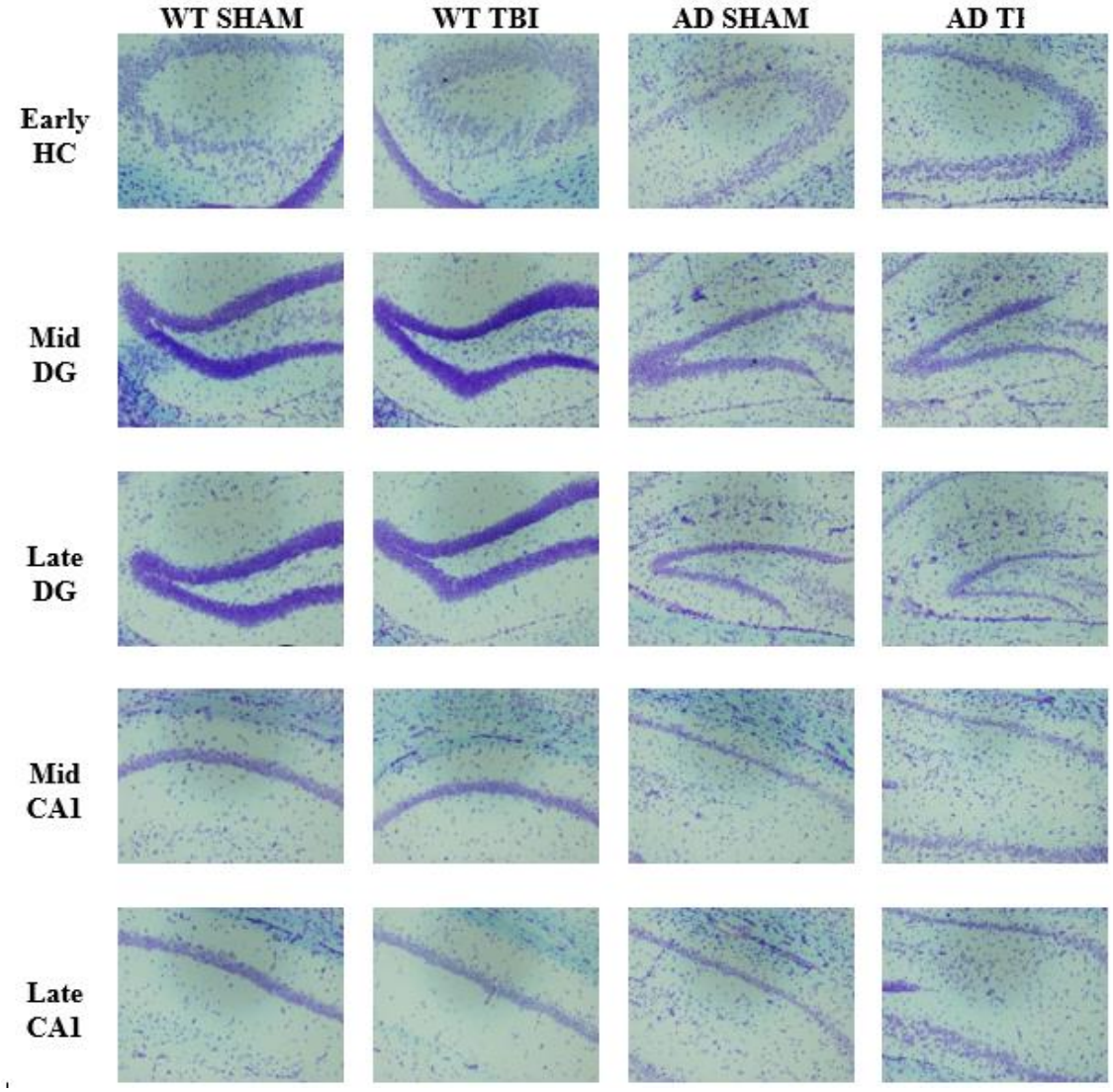

Figure 20: Cresyl-Violet Staining for Cell Bodies in Hippocampal Regions. Cresyl-violet staining for cell density revealed significantly lower cell density in AD mice compared to wt mice in the early HC ($p = 0.036$), mid DG ($p < 0.001$), mid CA1 ($p < 0.001$), late DG ($p < 0.001$), and late CA1 ($p < 0.001$). No significant effect of TBI was found ($p > 0.05$).

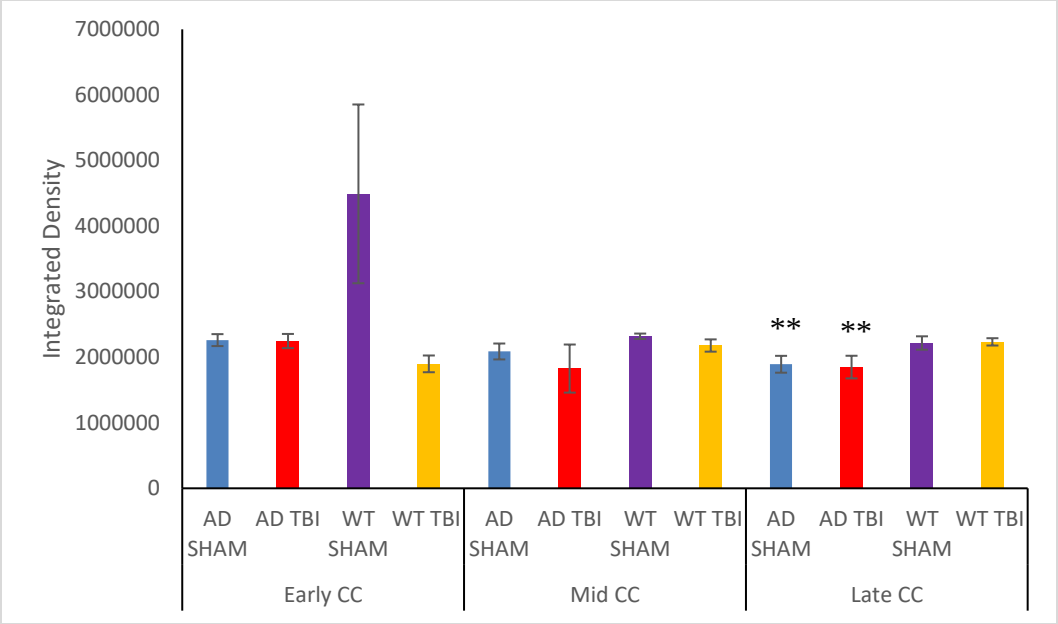

Figure 21: Integrated Density of White Matter at Midline Corpus Callosum. Average integrated density of white matter (±SEM) found at midline corpus callosum. A main effect of genotype was found in the late corpus callosum with AD type mice displaying significantly lower white matter density than wild type mice ($p = 0.01$). No significant difference of white matter density was found in the early ($p = 0.76$) or mid ($p = 0.329$) corpus callosum at the midline.

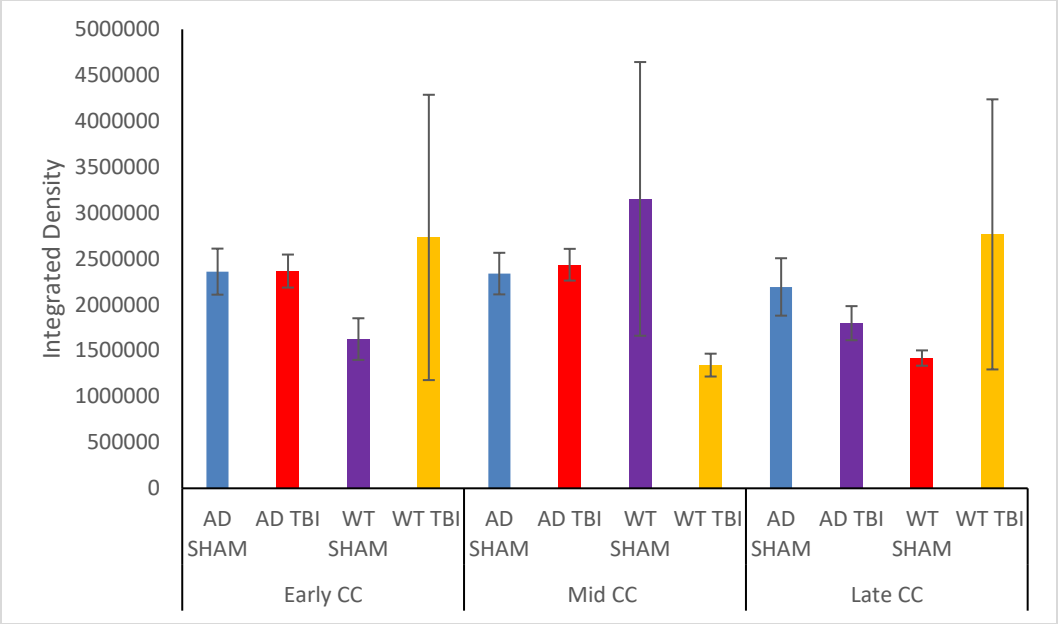

Figure 22: Integrated Density of Cell Bodies at Midline Corpus Callosum. Average integrated density of cell bodies (±SEM) found at midline corpus callosum. No significant difference of cell body density was found in the early (p = 0.62), mid (p = 0.437) or late (p = 0.639) corpus callosum at the midline.

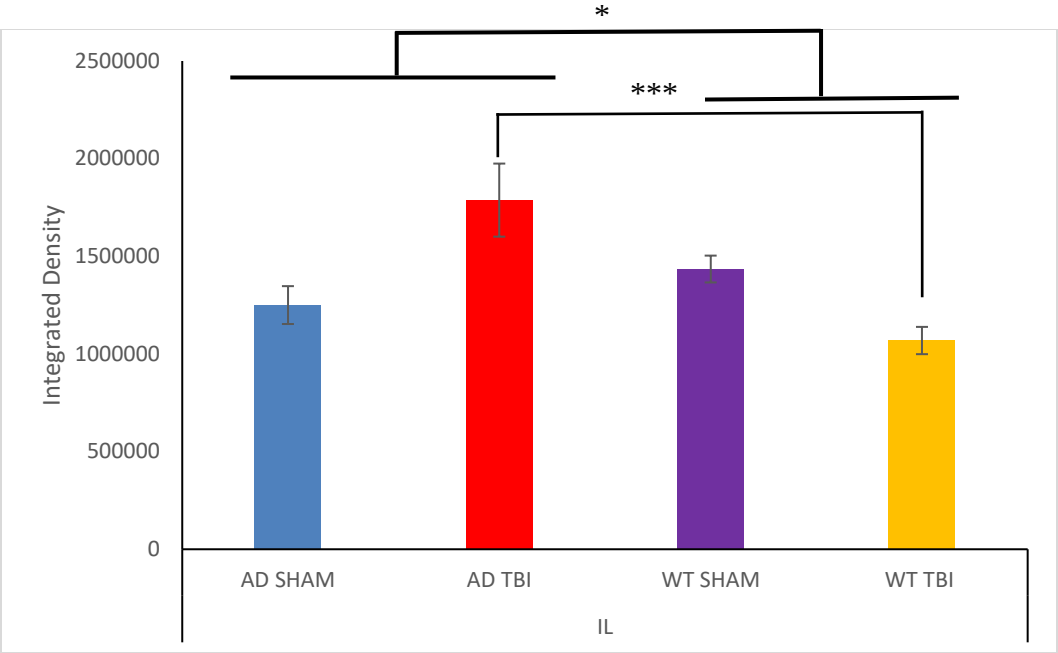

Figure 23: Integrated Density of Cell Bodies in Infralimbic Region.
Average integrated density of cell bodies (±SEM) found in the infralimbic region of the prefrontal cortex. A main effect of genotype was present with AD mice showing significantly higher integrated density of cell bodies ($p = 0.035$) compared to wt mice. A genotype*condition interaction was found with AD TBI mice showing significantly higher cell density than WT TBI mice ($p = 0.001$). * indicates significance at the $p < 0.05$ level, *** indicates significance at the $p = 0.001$ 1evel.

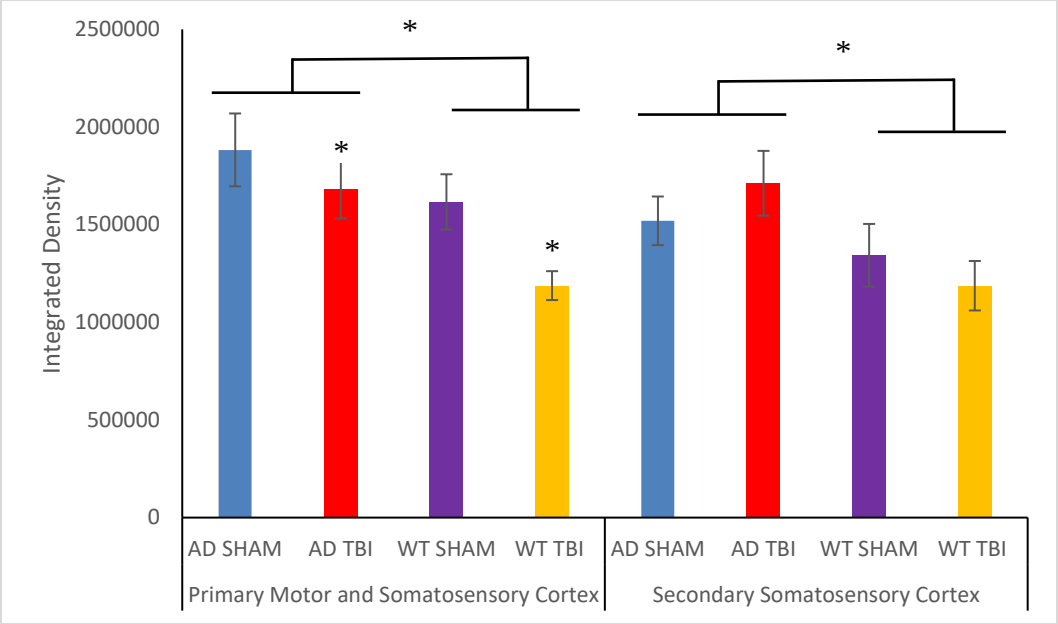

Figure 24: Integrated Density of Cell Bodies in Early Cortical Regions.
Average integrated density of cell bodies (±SEM) found at midline corpus callosum. A main effect of genotype was present with AD mice showing significantly higher integrated density of cell bodies in the primary motor and somatosensory cortex (p = 0.018) and in the secondary somatosensory cortex (p = 0.029) than wt mice. A TBI effect was present in the primary motor and somatosensory cortex, with rmTBI mice showing significantly lower integrated density of cell bodies (p = 0.044) than sham mice. * indicates significance at $p < 0.05$ level

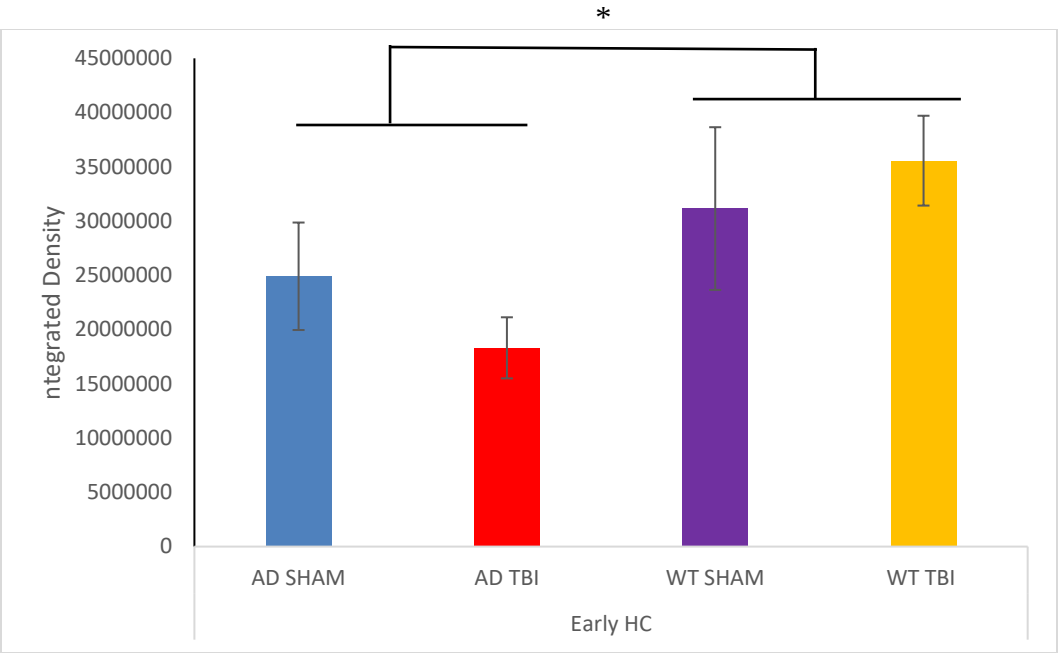

Figure 25: Integrated Density of Cell Bodies in Early Hippocampus.
Average integrated density of cell bodies (±SEM) found in early hippocampus. A main effect of genotype was present with AD mice showing significantly lower integrated density of cell bodies ($p = 0.036$) compared to wt mice. * indicates significance at the $p < 0.05$ level.

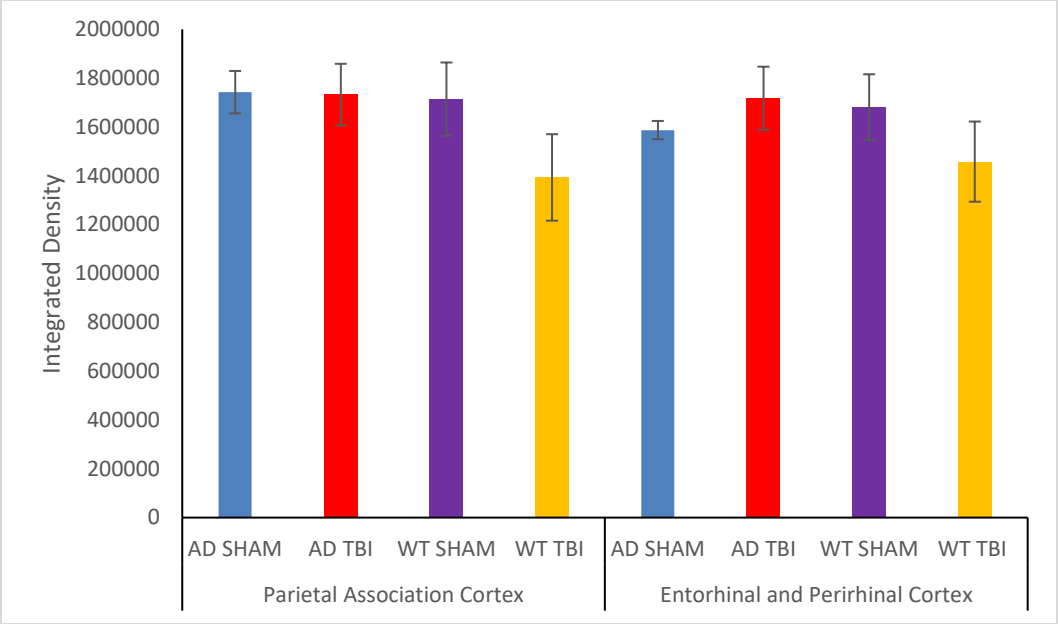

Figure 26: Integrated Density of Cell Bodies in Mid Cortical Regions.
Average integrated density of cell bodies (±SEM) found in mid cortical regions. There was no significant difference of cell body density in the parietal association cortex (p = 0.260) or in the entorhinal and perirhinal cortices (p = 0.489).

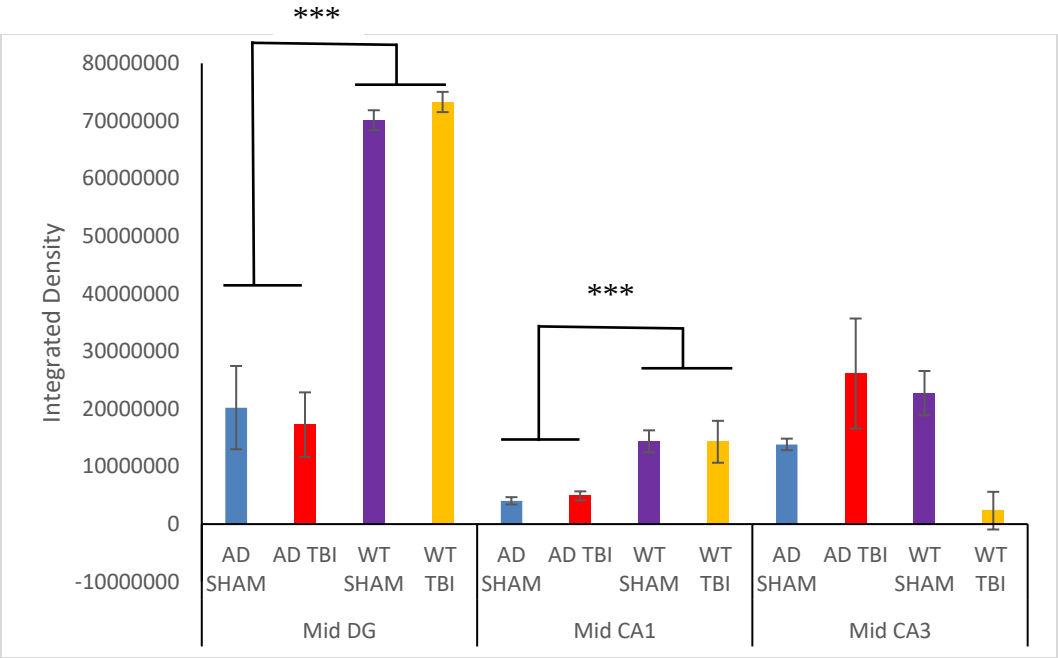

Figure 27: Integrated Density of Cell Bodies in Mid Hippocampus.
Average integrated density of cell bodies (±SEM) found in middle hippocampal regions. A main effect of genotype was present with AD mice showing significantly lower integrated density of cell bodies in the mid DG ($p < 0.001$) and in the mid CA1 ($p < 0.001$) compared to wt mice. No significant difference in cell body density was found in the mid CA3 ($p = 0.432$). *** indicates significance at the $p < 0.001$ level.

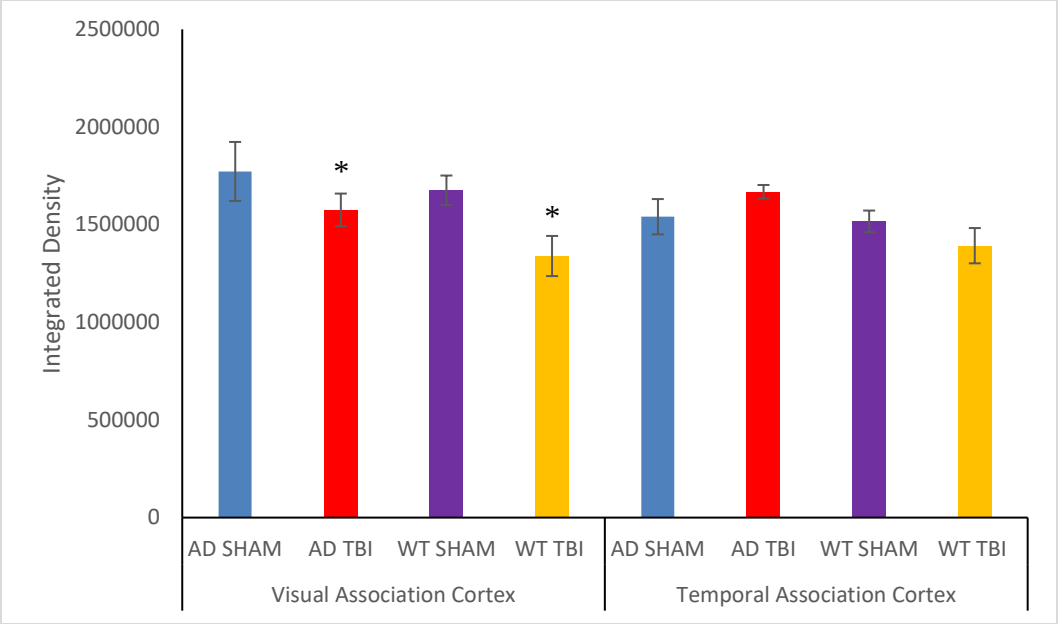

Figure 28: Integrated Density of Cell Bodies in Late Cortical Regions.
Average integrated density of cell bodies (±SEM) found in late cortical regions. A main effect of condition is present with TBI mice showing significantly lower integrated density of cell bodies in the visual association cortex ($p = 0.024$) compared to SHAM animals. No significant difference in cell body density was found in the temporal association cortex ($p = 0.098$). * indicates significance at the $p < 0.05$ level.

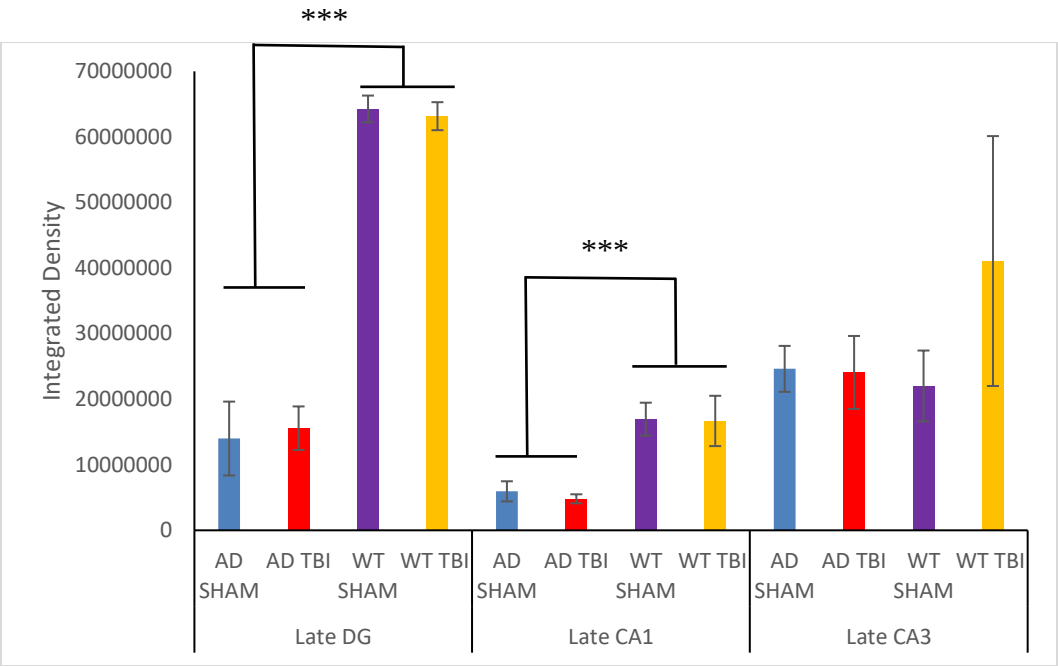

Figure 29: Integrated Density of Cell Bodies in Late Hippocampus.
Average integrated density of cell bodies (±SEM) found in the late hippocampus. A main effect of genotype is present with AD mice showing significantly lower integrated density of cell bodies in the late DG ($p < 0.001$) and in the late CA1 ($p < 0.001$) compared to wt mice. No significant difference in cell body density was found in the late CA3 ($p = 0.558$).

Table 1: Total Count of Amyloid Plaques, Tau Tangles, and Tau Tangle Size. Average totals of plaques, tangles and tangle size for each of the brain regions evaluated. Significantly more tau tangles were found in the IL, parietal association cortices, entorhinal and perirhinal cortices, mid DG, mid CA1, visual association cortex, late DG and late CA1 in mice that received rmTBI. Significantly larger tau tangles were found in the temporal association areas of mice that received rmTBI. There were no significant differences in number of amyloid plaques between groups. * indicates significance at the $p < 0.05$ level, ** indicates significance at the $p < 0.01$ level, *** indicates significance at the $p < 0.001$ level.

	Plaque Count		Tangle Count		Tangle Size	
Brain Region	AD SHAM	AD TBI	AD SHAM	AD TBI	AD SHAM	AD TBI
IL	0.03	0.05	163.5	249.1*	2047.1	2301.1
Primary Motor and Somatosensory Cortex	1.4	0.4	122	158.5	1698.3	1970.6
Secondary Somatosensory Cortex	0	0	146.8	185.7	1571.2	1619.7
Early HC	0.9	0.1	117.6	82	2810	1604.1
Parietal Association Cortices	2	0.6	131	316.6**	1360.2	1643
Entorhinal and Perirhinal Cortices	0	0.1	146.4	271***	1683.1	1929.8
Mid DG	0.5	0.5	54.8	89.6*	1328.1	1189.9
Mid CA1	0.4	0.3	52.3	105.1**	1354.1	1552.7
Mid CA3	0	0	92.5	128.1	1694.7	1544.5
Visual Association Cortex	2	1.8	92.3	192*	1525.8	1754.2
Temporal Association Areas	0	0	163	207.4	1708.9	2258.7*
Late DG	0.5	0.3	54.3	98.3***	1720.7	1423.4
Late CA1	0.5	0.2	52.7	86.5***	1999.3	1766.2
Late CA3	0.07	0	110.6	122	2013.8	1564.2

Table 2: Total Cell Density of All Brain Regions Assessed. Average total cell density across all brain regions assessed. * indicates a significant genotype effect at the $p < 0.05$ level, ** indicates a significant genotype effect at the $p < 0.01$ level, *** indicates a significant genotype effect at the $p < 0.001$ level, + indicates a significant condition effect, # indicates a significant interaction. Symbols are placed on the group with lower cell density. Numbers are rounded to the nearest thousand.

Brain Region	AD SHAM	AD TBI	WT SHAM	WT TBI
IL	1,250, 000	1,788,000	1,435,000*	1,068,000*#
Primary Motor and Somatosensory Cortex	1,883,000	1,682,000	1,617,000*	1,188,000*+
Secondary Somatosensory Cortex	1,520,000	1,712,000	1,343,000*	1,187,000
Early HC	24,914,000*	18,318,000*	31,153,000	35,569,000
Parietal Association Cortices	1,723,000	1,733,000	1,714,000	1,393,000
Mid DG	20,225,000***	17,264,000***	70,114,000	73,288,000
Mid CA1	4,040,000***	4,900,000***	14,361,000	14,291,000
Mid CA3	13,834,000	26,151,000	22,728,000	2,335,000
Visual Association Cortex	1,772,000	1,575,000	1,676,000	1,339,000*
Temporal Association Cortex	1,540,000	1,668,000	1,517,000	1,392,000
Late DG	13,997,000***	15,572,000***	64,268,000	63,159,000
Late CA1	5,942,000***	4,807,000***	16,958,000	16,678,000
Late CA3	24,623,000	24,069,000	22,011,000	41,066,000

Tau Tangles Normalized to Cell Density

Since NFTs occur intracellularly, number of tangles was then normalized to integrated cell density. An independent samples t-test was run on these values. This changed the number of regions showing significant changes. In cortical regions, there was a significant difference in the parietal association cortex ($t(8) = -4.491$, $p = 0.002$), in the entorhinal and perirhinal cortices ($t(8) = -3.093$, $p = 0.015$) and in the visual association cortex ($t(8) = -3.664$, $p = 0.006$) with AD TBI mice have a larger number tau tangles normalized to cell density. In hippocampal regions, only the mid CA1 region showed significance once values were normalized ($f(8) = -2.977$, $p = 0.018$), with AD TBI mice still showing more tau tangles once normalized to cell density. The mid DG, late DG and late CA1 no longer showed significant differences once tau tangle numbers were normalized to cell density.

CHAPTER FOUR: CONCLUSIONS

This study demonstrated the neuropathological changes that occur in a dual tg mouse model of AD following rmTBI. Eight-month-old hAPP/hTau mice that received rmTBI during adolescence display increased neurodegeneration in select brain regions. There were significantly more NFTs found in the IL, parietal association cortices, ERC and perirhinal cortex, visual association cortex, mid DG, mid CA1, late DG and late CA1 in mice who received rmTBI compared to SHAM mice. There were also significantly larger NFTs found in the temporal association area of rmTBI mice compared to SHAM mice. The distribution of tangles is similar to that seen by Braak and Braak (1991), with tangles showing up heavily in the ERC, HC and association cortices, sparing the primary motor and visual cortex. One number of tau tangles were normalized to cell density, the TBI effects were still seen in the cortical regions, but only the mid CA1 region of the hippocampus still showed significant differences in tangle formation. In contrast, in all brain regions assessed, there were no significant differences in amyloid plaque formation. Interestingly, while there were hundreds of NFTs found in each brain region, there was a very small number of amyloid plaques present.

The predominant theory of AD pathology development is the amyloid cascade hypothesis. This theory is a serial model that begins with an imbalance between Aβ production and clearance, leading to the accumulation of Aβ in the brain. According to the amyloid cascade hypothesis, Aβ accumulation is the primary influence of all resulting AD pathogenesis (Hardy & Selkoe, 2002; Karran, Merken, & Strooper, 2011). Genetic

mutations that cause an increase in pathogenic forms of amyloid lead to aggregation of toxic Aβ-42 oligomers and amyloid plaques. The neurotoxicity and synaptic toxicity of these oligomers and the synaptic disruption caused by plaque formation leads to PHF formation and NFT deposition (Hardy & Selkoe, 2002; Karran, Merken, & Strooper, 2011). This increasing neurodegeneration is what ultimately leads to neuronal dysfunction and cell death, causing dementia (Hardy & Selkoe, 2002). The amyloid cascade hypothesis has been supported through work in tg mice that overexpress both hAPP and htau, where tau-positive NFTs are increased compared to tg mice that only express htau (Hardy & Selkoe, 2002).

However, there are many concerns with the amyloid cascade hypothesis as being the only explanation for disease progression in both early-onset and late-onset AD. Early onset AD has heavy genetic influence, with mutations in the presenilin 1 and 2 genes causing a disruption in amyloid processing. However, genetic impact on late-onset AD comes through the APOE 4 allele, which does not influence amyloid processing as heavily as the presenilin mutations and the presence of the APOE e4 allele, while increasing the risk for development of AD, does not always lead to an AD diagnosis. (Hardy & Selkoe, 2002; Karren et al., 2011). Another problem with amyloid cascade hypothesis is the number of amyloid deposits does not correlate with the degree of cognitive impairment (Hardy & Selkoe, 2002). Additionally, all therapeutics that target Aβ have failed in clinical trials (Karran et al., 2011). During autopsy, human patients who were immunized against Aβ-42 showed almost a complete reduction in amyloid pathology, while tau was still heavily present, and there was no slowing or rescuing of

behavioral deficits (Small & Duff, 2008). Comparatively, reduction of tau in hAPP/htau mice rescued behavioral deficits (Karran et al., 2011). Mutations in the tau gene can cause frontotemporal dementia, with tau pathology similar to that seen in AD, without the presence of Aβ plaques (Karren et al., 2001).

In response to these problems, a dual pathway hypothesis was proposed to explain disease progression that may not be a direct result of amyloid pathology. This model suggests that Aβ accumulation and increase in tau hyperphosphorylation can occur by separate but parallel mechanisms that may be driven by a common molecular deficit. Both Aβ accumulation and tau hyperphosphorylation lead to synapse loss, cell death, and eventually dementia (Small & Duff, 2008). The dual pathway model proposes that for late-onset AD, the APOE 4 allele is responsible for the pathological changes seen in AD. APOE 4 has been shown to decrease astroglia clearance of Aβ, leading to Aβ accumulation(Small & Duff, 2008). It also has the greatest effect, compared to APOE 2 and APOE 3 in activation glycogen kinase 3 (GSK-3) which phosphorylates tau (Small & Duff, 2008). APOE 4 may also bind to tau to block phosphorylation sites and APOE 4 binds the least strongly of the three alleles, leaving tau open to hyperphosphorylation by GSK-3 (Small & Duff, 2008) and leading to tau pathology and NFT formation.

With similar behavioral deficits and neuropathology, TBI studies also give support to the possibility of dual mechanisms, as in many cases there is pathogenic tau with an absence of amyloid (McKee et al., 2009), providing evidence that amyloid pathology is not an essential prerequisite to tau pathology. Increases in NFT formation independent of amyloid plaque deposition is a common feature of rmTBI. Mice in this

study that experienced rmTBI had further progressed tau pathology than amyloid pathology in several key brain areas related to memory, lending support to the dual pathway model. This is an expected result, as multiple studies have shown that while an increase in NFTs and phosphorylated tau is a core defining feature of CTE, the presence of amyloid plaques is less common (Faden & Loane, 2014; Johnson et al., 2012; Kane et al., 2011; McKee et al., 2009).

In humans who have experienced rmTBI or who were diagnosed with CTE post-mortem, Aβ was only found in 30-45% of cases, with diffuse plaques appearing more frequently than neuritic or vascular plaques, although plaque formation remained inconsistent between cases (Edwards, Moreno-Gonzalez & Soto., 2016). Comparatively, tau immunoreactive NFTs in the superficial cortical layers are extensively seen following TBI with a higher density and wider distribution of tangles in those surviving more than one year after injury (Johnson et al., 2012; McKee et al., 2009). Animal models of rmTBI also show increased pathologic tau. Increased total tau immunoreactivity following TBI is present in the amygdala and CA1 region of the HC (Tran et al., 2011). Increased levels of phosphorylated tau have also been found following TBI in both wt and AD-type mice, with level of tau accumulation dependent on injury severity (Kane et al., 2011; Tran et al., 2011). Mice from the current study also showed increased total tau and phosphorylated tau in rmTBI mice compared to SHAM mice as seen through Western Blots (Craven, 2019). These increases in total tau and phosphorylated tau can lead to increased NFT formation (Tran et al., 2011), which was also seen in this study.

While the neuritic plaques of AD are not as frequently seen following rmTBI, diffuse plaques, pathologic amyloid, and toxic amyloid oligomers may be present. In humans, abundant diffuse amyloid plaques were found in individuals with CTE (McKee et al., 2009: Roberts et al., 1990), however, these diffuse plaques had no association with dystrophic neurites or reactive glial cells and are unable to be visualized through the use of Congo Red stain (Hardy & Allsop., 1991; Roberts et al 1990), which may explain why so few plaques were seen in this study. Following rmTBI, APP processing is disrupted (Blasko et al., 2004; Itoh et al., 2009; Lauer et al., 2001), causing an increase in APP expression in cortical neurons from 1-90 days post-injury (Itoh et al., 2009), as well as an increase in beta-secretase-1, which leads to an overproduction of pathogenic amyloid (Blasko et al., 2004). Toxic amyloid oligomers have also been found following rmTBI (Faden & Loane, 2014; Uryu et al., 2012,), with rmTBI accelerating the production of Aβ-40 and 42 and the accumulation of both soluble and insoluble oligomers (Uryu et al., 2002). Aβ deposition was also increases after rmTBI in the HC, frontal, cingulate and perihippocampal cortices but only at 12 months of age (Uryu et al., 2002).

While mice in this study did not show neuritic plaque formation, more research is needed to determine if other amyloid pathology present. Perhaps in this rmTBI model, there were diffuse plaques present that were not visualized through Congo Red staining or toxic oligomers contributing to the other neurodegeneration. Soluble oligomers of Aβ may be responsible for synaptic dysfunction, synaptotoxicity, and inhibition of long-term potentiation in the HC (Hardy & Selkoe., 2002; Jin et al., 2011., Serrano-Pozo et al., 2011). Higher levels of toxic, soluble, Aβ oligomers mainly composed of Aβ-42 were

correlated with more severe cognitive impairment and increased Braak stage and have been shown to induce tau hyperphosphorylation, disrupt microtubules, and induce neurofibrillary changes (Jin et al., 2011). Even with plaques absent, Aβ-42 has been shown to increase tau pathology. As such, more research is needed to see if there were pathologic amyloid changes outside of neuritic plaque formation in response to rmTBI.

Significant differences in cell density in response to both genotype and rmTBI administration were also found. Cresyl-Violet staining showed genotype effects in both cortical and hippocampal brain regions. In hippocampal regions, there was significantly lower cell body density in AD mice compared to wt mice in the early HC, mid DG, mid CA1, late DG and late CA1. Conversely, in cortical regions, there was higher cell body density in AD mice than in wt mice in the IL, secondary somatosensory cortex and the primary and secondary motor cortex. Typically in AD, neuronal loss and synapse loss parallel tangle formation (Serrano-Pozo et al., 2011). While this was true for the HC, which saw both significant tangle formation and cell loss, that trend did not continue in cortical regions, where the IL had significant tangle formation but AD mice had greater cell density than wt mice. Other cortical regions that showed significant NFT deposition, such as the ERC and perirhinal cortex, and the parietal and visual association cortices also did not show cell loss in AD mice. Rather, the somatosensory and motor cortices had greater cell density in AD mice than wt mice. This result was unexpected as studies using AD-type tg mice show neuron loss (Serrano-Pozo, Jin et al, Edwards 2016).

There were TBI effects on cell density seen in cortical regions. In the primary and secondary motor cortex, and in the visual association cortex, mice who receive rmTBI

had significantly lower cell density than SHAM mice. In the infralimbic regions, AD TBI mice had significantly lower cell density than wt TBI mice. There was no significant rmTBI effect on cell density in hippocampal regions. While cell loss is a common feature in AD mice (Serrano-Pozo et al., 2011), studies on rmTBI have shown mixed results. In humans with CTE, there is neuronal loss in the HC and cerebral cortex, accompanied by neurofibrillary degeneration (McKee et al., 2009) and in mice, neuronal loss is most severe in the HC, ERC, and amygdala (Edwards et al., 2016). Many other mouse models of rmTBI, however, showed no cell loss (Kane et al., 2011; Luo et al., 2014; Mouzon et al., 2012; Uryu et al., 2002). These models used wt mice and sacrificed mice one month after injury (Kane et al., 2011; Mouzon et al., 2012), only looked at the HC and not cortical regions (Luo et al., 2014) or used a mouse model of AD that only expressed amyloid (Uryu et al., 2002), which may explain some of the differences that were seen. Mice in this study were aged to 8 months—5 months post-injury—and expressed both amyloid and tau. Previous studies have shown that mice only expressing amyloid often do not show extensive neuronal loss, perhaps due to a lack of human tau (Hardy & Selkoe, 2002). As rmTBI mouse models have shown conflicting results due to methodological differences, more research is needed with this mouse model and rmTBI method to explain the variations in cell density seen here.

Inflammation may play a role in where neurodegeneration was seen. The brain regions that did see an rmTBI effect were regions closest to the site of initial injury. Previous studies showed that following rmTBI glial fibrillary acidic protein (GFAP) was only found in cortical regions underlying the initial impact site and not at all other brain

regions (Mouzon et al., 2012). The TBI method used in this study was mild, and damage may not have been severe enough to reach more distant brain regions. Therefore, cell loss may not be as extensive or widespread as it would be with a more severe injury. Additionally, a previous study using these mice found an increase in GFAP in AD mice, which saw cell loss in the hippocampus (Craven, 2019). Inflammation and microglial activation following TBI are likely chronic, and axonal degeneration and tissue atrophy associated with inflammation may contribute to ongoing neurodegeneration (Johnson et al., 2012). Perhaps cell loss was only seen in these regions as a result of GFAP expression in the cortex under the injury site. More research is needed to determine if GFAP responses in mice in response to this rmTBI method was localized to regions closest to the impact site, or diffuse throughout the brain.

This study used a novel mouse model that crossed an hAPP/J20 mouse with an hTau/rTg4510 mouse to develop both human amyloid and human tau. The background strains of this mouse model both show age related neuron loss in the HC (Spires et al, 2006; Wright et al, 2013). By 8.5 months, rTg4510 mice show over 80% cell loss in the CA1 and DG regions, 69% in the CA2/CA3 region and 52% in the cortex. Cell loss is not seen in the cortex until 8.5 months (Spires et al, 2006). rTg4510 mice begin to develop NFTs between 2.5 and 7 months of age, but tangle formation does not always correlate with cell loss. In the HC, cell loss is seen before the formation of tangles, and in cortical regions, although 25% of neurons expressed tau immunoreactivity, there was no significant loss of neurons prior to 8.5 months (Spires et al, 2006). In the hAPP/J20 model, neuronal loss is severe in the HC beginning at 12 weeks and spreads to the

cerebral cortex during disease progression (Wright et al, 2013). The pronounced cell loss in the HC in both models parallels the cell loss seen in the current study. Also similar to this study, hAPP/J20 mice do not express cell loss in the CA3 region of the HC (Wright et al, 2013). In hAPP/J20 mice, the extent of neuron loss correlated with age and number of activated microglia (Wright et al., 2013). Formation of plaques and oligomeric Aβ were the last changes seen at 36 weeks, with a significant number of plaques found in the HC at 36 weeks (Wright et al., 2013), which was not supported by the current study, as fewer than 10 plaques were seen in each region.

Although there was extensive neurodegeneration seen, particularly NFT formation, these mice performed several behavioral assays with no significant deficits. In a previous study mice completed several behavioral assays and while there were genotype effects, with AD mice showing memory impairment compared to tg mice in the MWM, as well as behavioral disinhibition in the elevated zero maze, there were few effects of rmTBI (Craven, 2018). AD rmTBI mice showed increased risk-taking behavior on the elevated zero maze, as seen through more head dips, and had disrupted circadian rhythms at 4 months of age (Craven, 2019f) compared to AD SHAM mice. These behavioral deficits were also seen in other studies, with rmTBI mice showing no learning and memory deficits (Laurer et al., 2014), but rather, demonstrating increased risk-taking behavior and sleep disturbances (Petraglia et al., 2014). An interesting behavioral result seen was AD mice were significantly faster and ran significantly further distances in open field testing than wt mice (Craven, 2019). This behavior helps to explain the result that AD mice showed higher cell density in the motor cortex than wt mice. Additionally,

hAPP/J20 mice demonstrate increased hyperactivity beginning at 16 weeks (Wright et al, 2013), which may also explain the increased cell density in the motor cortex. While there was significant neuropathology in AD mice who received rmTBI in brain regions important for learning and memory, there were not many behavioral deficits seen compared to other AD-type mice. The AD mice may have already have such progressed neurodegeneration that a distinction of behavioral deficits can no longer be made, or the rmTBI model that was used is so mild that it does not cause long-term learning and memory deficits. As wild-type animals used in this study also did not show a significant learning and memory problems in response to rmTBI, it is likely that the TBI model was too mild to show extensive behavioral deficits.

Overall, this study provides evidence that rmTBI in adolescence progressed the neuropathology of AD later in life. TBI induced progression of AD neuropathology is not necessarily mediated by the amyloid cascade hypothesis, rather, it is likely worsened through dual pathways. However, this progression was not severe enough to make behavioral deficits caused by rmTBI distinguishable from those resulting from AD pathology alone. This may be due to the injury occurring during adolescence, where the brain is more plastic and had time to recover from the injury with no long-term behavioral deficits. It may also be due to the mild nature of the injury; there may not have been a great enough impact to cause long-term behavioral deficits, even though there was further progressed neuropathology. Future research is needed to determine the mechanism behind increased tau accumulation and whether diffuse plaques or toxic amyloid oligomers were present as a result of this rmTBI model. Research is also needed

to better explain the higher cell density seen in cortical regions of AD mice in this mouse model.

REFERENCES

Anderson, V., Brown, S., Newitt, H., & Hoile, H. (2011). Long-term outcome from childhood traumatic brain injury: Intellectual ability, personality, and quality of life. *Neuropsychology, 25*(2), 176-184. doi: 10.1037/a0021217

Armstrong, R. C., Mierzwa, A. J., Marion, C. M., & Sullivan, G. M. (2016). White matter involvement after TBI: Clues to axon and myelin repair capacity. *Experimental Neurology, 275(3),* 328-333. https://doi.org/10.1016/j.expneurol.2015.02.011

Blasko, I., Beer, R., Bigl, M., Apelt, J., Franz, G., Rudzki, D. … Schliebs, R. (2004). Experimental traumatic brain injury in rats stimulates the expression, production and activity of Alzheimer's disease β-secretase (BACE-1). *Journal of Neural Transmission, 111*(4), 523-536. https://doi.org/10.1007/s00702-003-0095-6

Bolton, A. N., & Saatman, K. E. (2014). Regional neurodegeneration and gliosis are amplified by mild traumatic brain injury repeated at 24-hour intervals. *J Neuropathol Exp Neurol, 73*(10), 933-947. doi 10.1097/NEN.0000000000000115

Bondi, M. W., Edmonds, E. C., & Salmon, D. P. (2017). Alzheimer's disease: Past, present, and future. *Journal of International Neuropsychological Society, 23,* 818-831. doi: 10.1017/S135561771700100X

Braak, H., & Braak, E. (1991). Neuropathological stageing of Alzheimer-related changes. *Acta Neuropathologica, 82*(4), 239-259 doi: 10.1007/bf00308809

Braun, M., Vaibhav, K., Saad, N. M., Fatima, S., Vender, J. R. Baban, B. … Dhandapani, K. M. (2017). White matter damage after traumatic brain injury: A role for

damage associated molecular patterns. *BBA- Molecular Basis of Disease, 1863*(10), 2614-2626. https://doi.org/10.1016/j.bbadis.2017.05.020

Bruns, F., & Hauser, A. (2003). The epidemiology of traumatic brain injury: A review. *Epilepsia, 44*(s10), 2-10. https://doi.org/10.1046/j.1528-1157.44.s10.3.x

Carbonell, W. S. & Grady, M. S. (1999). Regional and temporal characterization of neuronal, glial, and axonal response after traumatic brain injury in the mouse. *Acta Neuropathologica, 98,* 396-406. http://doi.org/10/1007/s004010051100

Dia, M. H., Zheng, H., & Zhang, Y. (2017). The genes associated with early-onset Alzheimer's disease. *Oncotarget, 9*(19), 15132-15143. doi: 10.18632/oncotarget.23738

Edwards III, G. Moreno-Gonzalez, I., & Soto, C. (2016). Amyloid-beta and tau pathology following repetitive mild traumatic brain injury. *Biochemical and Biophysical Research Communications, 483*(4), 1137-1142. https://doi.org/10.1016/j.bbrc.2016.07.123

Craven, K. M. (2019). Repetitive mild traumatic brain injury exacerbates the progression of Alzheimer's disease in a mouse model (Publication No. 13865592). [Doctoral dissertation, George Mason University]. ProQuest Dissertations Publishing.

Faden, A. I., & Loane, D. J. (2015) Chronic neurodegeneration after traumatic brain injury: Alzheimer disease, chronic traumatic encephalopathy, or persistent neuroinflammation. *Neurotherapeutics, 12*(1), 143-150. doi: 10.1007/s13311-014-0319-5

Franklin, K. B. J. & Paxinos, G. (2008). The Mouse Brain in Stereotaxic Coordinates (Third Edition). Elsevier.

Grundke-Iqbal, I., Iqbal, K., Tung, Y. C., Quinlan, M., Wishiewski, H. M., & Binder, L. I. (1986). Abnormal phosphorylation of the microtubule-associated protein τ (tau) in Alzheimer's cytoskeletal pathology. *Proceedings of the National Academy of Sciences of the United States of America, 83*(13), 4913-4917. doi: 10.1073/pnas.83.13.4913

Haass, C., & Selkoe, D. J. (1993). Cellular processing of β-amyloid precursor protein and the genesis of amyloid β-peptide. *Cell, 75*(6), 1039-1042. https://doi.org/10.1016/0092-8674(93)90312-E

Hardy, J., & Allsop, D. (1991) Amyloid deposition as the central even in the aetiology of Alzheimer's disease. *Trends in Pharmacological Sciences, 12*(10), 383-388. Retrieved from https://www.ncbi.nlm.nih.gov/pubmed/1763432

Hardy, J., & Selkoe, D. J. (2002). The amyloid hypothesis of Alzheimer's disease: Progress and problems on the road to therapeutics. *Science, 297*(5590), 353-356. doi: 10.1126/science.1072994

Itoh, T., Satou, T., Nishida, S., Tsubaki, M., Hashimoto, S., & Ito, H. (2009). Expression of amyloid precursor protein after rat traumatic brain injury. *Neurological Research, 31*(1), 103-109. doi: 10.1179/016164108X323771

Jin, M., Shepardson, N., Yang, T., Chen, G., Walsh, D., & Selkoe, D. J. (2011). Soluble amyloid β-protein dimers isolated from Alzheimer cortex directly induce tau hyperphosphorylation and neuritic degeneration. *Proceedings of the National*

Academy of Sciences of the United States of America, 108(14), 5819-5824. doi: 10.1073/pnas.1017033108

Johnson, V. E., Stewart, W., & Smith, D. H. (2012). Widespread tau and amyloid-beta pathology many years after a single traumatic brain injury in humans. *Brain Pathology, 22*(2), 142-149. doi: 10.1111/j.1750-3639.2011.00513.x

Kane, M. J., Angoa-Perez, M., Briggs, D. I., Viano, D. C., Kreipke, C. W., & Kuhn, D. M. (2011). A mouse model of human repetitive mild traumatic brain injury. *Journal of Neuroscience Methods, 203*(2012), 41-49. doi: 10.1016/j.jneumeth.2011.09.003

Karran, E., Merken, M. & De Strooper, B. (2011). The amyloid cascade hypothesis for Alzheimer's disease: An appraisal for the development of therapeutics. *Nature Reviews Drug, 10*, 698-712. doi: 10.1039/nrd3505

Kumar, A., Singh, A., & Ekavali. (2015). A review on Alzheimer's disease an its management: An update. *Pharmacological Reports, 67*(2), 195-203. doi: 10.1016/j.pharep.2014.09.004

Langlois, J. A., Rutland-Brown, & Wald, M. M. (2006). The epidemiology and impact of traumatic brain injury: A brief overview. *The Journal of Head Trauma Rehabilitation, 21*(5), 375-378. Retrieved from https://journals.lww.com/headtraumarehab/Fulltext/2006/09000/The_Epidemiology_and_Impact_of_Traumatic_Brain.1.aspx

Laurer, H. L., Bareyre, F. M., Lee, V. M. Y. C., Trojanowski, J. Q., Longhi, L., Hoover, R., … McIntosh, T. K. (2001). Mild head injury increasing the brain's

vulnerability to a second concussive impact. *Journal of Neurosurgery, 95*(5), 859-870. doi: 10.3171/jnas.2001.95.5.0859

Lippi, S. L. P., Smith, M. L., & Flinn, J. M. (2018). A novel hAPP/htau mouse model of Alzheimer's disease: Inclusion of APP with tau exacerbates behavioral deficits and zinc administration heightens tangle pathology. *Frontiers in aging neuroscience, 10*(382). doi: 10.3389/fnagi.2018.00382

Luo, J., Nguyen, A., Villeda, S., Zhang, H., Zhaoqing, D., Lindsay, D. ... Wyss-Coray, T. (2014). Long-term cognitive impairments and pathological alteration in a mouse model of repetitive mild traumatic brain injury. *Frontiers in Neurology, 5*. doi: 10.3389/fneur.2014.00012

Lye, T. C., & Shores, E. A. (2000). Traumatic brain injury as a risk factor for Alzheimer's disease: A review. *Neuropsychology Review, 10*(2), 115-129. https://doi.org/10.1023/A:1009068804787

McGowan, E., Eriksen, J., & Hutton, M. (2006). A decade of modeling Alzheimer's disease in transgenic mice. *Trends in Genetics, 22*(5), 281-288. doi: 10.1016/j/tig/2006/03.007

McKee, A. C., Cantu, R. C., Nowinski, C. J., Hedley-Whyte, T., Gavett, B. E., Budson, A. E., … Stern, R. A. (2009). Chronic traumatic encephalopathy in athletes: Progressive tauopathy after repetitive head injury. *Journal of Neuropathology and Experimental Neurology, 68*(7), 709-735. doi: 10.1097/NEN.0b013e3181a9d503

McKinlay, A., Grace, R. C., Horwood, L. J., Fergusson, D. M., Ridder, E. M., & MacFarlane, M. R. (2009). Prevalence of traumatic brain injury among children,

adolescents and young adults: Prospective evidence from birth cohort. Brain Injury, 22(2), 175-181. https://doi.org/10.1080/02699050801888824

Menon, D. K., Schwab, K., Wright, D. W., Maas, A. I., & Demographics and Clinical Assessment Working Group of the International and Interagency Initiative toward Common Data Elements for Research on Traumatic Brain Injury and Psychological Health. (2010). Position statement: definition of traumatic brain injury. *Archives of Physical Medicine and Rehabilitation, 91*(11), 1637–1640. doi:10.1016/j.apmr.2010.05.017

Mouzon, B., Chaytow, H., Crynen, G., Bachmeier, C., Stewart, J., Mullan, M., … Crawford, F. (2012). Repetitive mild traumatic brain injury in a mouse model produces learning and memory deficits accompanied by histological changes. *Journal of Neurotrauma, 29*(18), 2761-2773. doi: 10.1089/neu.2012.2498

Nasrabady, S. E., Rizvi, B., Goldman, J. E., & Brickman, A. M. (2018). White matter changes in Alzheimer's disease: A focus on myelin and oligodendrocytes. *Acta Neuropathologica Communications, 6*(22). https://doi.org/10.1186/s40478-018-0515-3

Petraglia, A. L., Plog, B. A., Dayawansa, S., Chen, M., Danshaw, M. L. Czerniecka, K. ... Huang, J. H. (2014). The spectrum of neurobehavioral sequelae after repetitive mild traumatic brain injury: a novel mouse model of chronic traumatic encephalopathy. *Journal of Neurotrauma, 31*(13), 1211-1224. doi: 10.1089/neu.2013.3255

Popescu, C., Anghelescu, A., Daia, C., & Onose, G. (2015). Actual data on epidemiological evolution and prevention endeavors regarding traumatic brain injury. *Journal of Medicine and Life, 8*(3), 272-277. Retrieved from https://www.ncbi.nlm.nih.gov/pmc/articles/PMC4556905/

Rieckmann, A., Van Dijk, K. R. A., Sperling, R. A., Johnson, K. A., Buckner, R. L., & Hedden, T. (2016). Accelerated decline in white matter integrity in clinically normal individuals at risk for Alzheimer's disease. *Neurobiology of Aging, 42*, 177-188. https://doi.org/10.1016/j.neurobiolaging.2016.03.016

Roberts, G. W., Allsop, D., & Bruton, C. (1990). The occult aftermath of boxing. *Journal of Neurology, Neurosurgery, and Psychiatry, 53*(5), 373-378. doi: 10.1136/jnnp.53.5.373

Serrano-Pozo, A., Frosch, M. P., Masliah, E., & Hyman, B. T. (2011). Neuropathological alterations in Alzheimer disease. Cold Spring Harbor Perspectives in Medicine, 1(1). doi: 10.1101/cshperspect.a006189

Small, S. A., & Duff, K. (2008). Linking Aβ and tau in late-onset Alzheimer's disease: A dual pathway hypothesis. *Neuron, 60*(4), 534-542. doi: 10.1016/j.neuron.2008.11.007

Spires, T. L., Orne, J. D., SantaCruz, K., Pitstick, R., Carlson, G. A., Ashe, K. H., & Hyman, B. T. (2006). Region-specific dissociation of neuronal loss and neurofibrillary pathology in a mouse model of tauopathy. *The American Journal of Pathology, 168*(5), 1598-1607. doi: 10.2353/ajpath.2006.050840

Sun, A., Nguyen, X., U., & Bing, G. (2002). Comparative analysis of an improved thioflavin-S stain, gallyas silver stain, and immunohistochemistry for neurofibrillary tangle demonstration on the same sections. *Journal of Histochemisty and Cytochemisty, 50*(4), 463-472. doi: 10.1177/002215540205000403

Tran, J. T. T., Laferla, F. M., & Holtzman, D. M. (2011). Controlled cortical impact traumatic brain injury in 3xtg-AD mice causes acute intra-axonal amyloid accumulation and independently accelerates the development of tau abnormalities. *The Journal of Neuroscience, 31*(26), 9513-9525 doi: 10.1523/JNEUROSCI.0858-11.2011

Uryu, K., Laurer, H., MnIntosh, T., Pratico, D., Martinez, D., Leight, S., … Trojanowski, J. Q. (2002). Repetitive mild brain trauma accelerates Aβ deposition, lipid peroxidation, and cognitive impairment in a transgenic mouse model of Alzheimer amyloidosis. *The Journal of Neuroscience, 22*(2), 446-454. https://doi.org/10.1523/JNEUROSCI.22-02-00446.2002

Weingarten, M. D., Lockwood, A. H., Hwo, S. Y., & Kirschner, M. W. (1975). A protein factor essential for microtubule assembly. *Proceedings of the National Academy of Sciences of the United States of America, 72*(5), 1858-1862. doi: 10.1073/pnas.72.5.1858

Winston, C. N., Noel, A., Neustadtl, A., Parsadanian, M., Barton, D. J., Chellappa, D. … Burns, M. P. (2016). Dendritic spine loss and chronic white matter inflammation

in a mouse model of highly repetitive head trauma. *The American Journal of Pathology, 186*(3), 552-567. https://doi.org/10.1016/j.ajpath.2015.11.006

Wright, A. L., Zinn, R., Hohensinn, B., Konen, L. M., Beynon, S. B., Tan, R. P. ... Vissel, B. (2013). Neuroinflammation and neuronal loss precede Aβ plaque deposition in the hAPP-J20 mouse model of Alzheimer's disease. PLoS One, 8(4). doi:10.1371/journal.pone.0059586

Xiong, Y., Mahmood, A., & Chopp, M. (2013). Animal models of traumatic brain injury. *Nature Reviews Neuroscience, 14*(2), 128-142. doi: 10.1038/nm3407

BIOGRAPHY

Rachel Barkey graduated from Franklin Regional High School in Murrysville, Pennsylvania in 2013. She received her Bachelor of Science from Messiah College in Mechanicsburg, PA in 2016. She was employed as a Milieu Therapist at Western Psychiatric Institute and Clinic in Pittsburgh, PA for one year before beginning the Master of Arts in Psychology with a concentration in Cognitive and Behavioral Neuroscience program at George Mason University in 2018.